



MODERN APPROACHES IN APPLIED MECHANICAL ENGINEERING- 2025

Edited By Prof. Dr. Kamal BOUZID

ISBN: 979-8-89695-198-8

DOI: 10.5281/zenodo.17362897

October / 2025 İstanbul, Türkiye



Copyright © Haliç Yayınevi

Date: 15.10.2025

Halic Publishing House İstanbul, Türkiye www.halicyayinevi.com

All rights reserved no part of this book may be reproduced in any form, by photocopying or by any electronic or mechanical means, including information storage or retrieval systems, without permission in writing from both the copyright owner and the publisher of this book.

© Halic Publishers 2025

The Member of International Association of Publishers

The digital PDF version of this title is available Open Access and distributed under the terms of the Creative Commons Attribution-Non-Commercial 4.0 license (http://creativecommons. org/licenses/by-nc/4.0/) which permits adaptation, alteration, reproduction and distribution for noncommercial use, without further permission provided the original work is attributed. The derivative works do not need to be licensed on the same terms.

adopted by Esma AKSAKAL ISBN: 979-8-89695-198-8

Copyright © 2025 by Halic Academic Publishers All rights reserved

MODERN APPROACHES IN APPLIED MECHANICAL ENGINEERING

EDITOR

Prof. Dr. Kamal BOUZID

AUTHORS

Prof. Dr. Kamal BOUZID

Asst. Prof. Mohd Saad SALEEM

Abdelileh MABROUK

Saimah KHAN

Lahoucine BELARCHE

Mohamed BOUNOUIB

Ali SIADI

Btissam ABOURIDA

Hassan HADI

TABLE OF CONTENTS

PREFACE	i
CHAPTER 1	
LYAPUNOV-BASED CONTROL OF MAGNET	TIC GEAR
SYSTEMS: STABILITY ANALYSIS USING BA	ARBALAT'S
LEMMA	
Abdelileh MABROUK	1
CHAPTER 2	
ADVANCEMENTS IN POWERTRAIN ARCHI	TECTURES AND
ENERGY MANAGEMENT STRATEGIES FO	R ELECTRIC AND
HYBRID VEHICLES: A MECHANICAL ENGI	INEERING
PERSPECTIVE	
Asst. Prof. Mohd Saad SALEEM	
Saimah KHAN	19
CHAPTER 3	
NANOFLUIDS (WATER + COPPER) OPTIMIS	
MIXED CONVECTION COOLING OF AN EL	ECTRONIC
COMPONENT IN A 3D CAVITY	
Prof. Dr. Kamal BOUZID	
Lahoucine BELARCHE	
Mohamed BOUNOUIB	
Ali SIADI	
Btissam ABOURIDA	
Hassan HADI	43

PREFACE

This volume presents three forward-looking chapters that tackle key challenges in control systems, automotive engineering, and thermal management. The first, Lyapunov-Based Control of Magnetic Gear Systems, applies nonlinear control theory and Barbalat's Lemma to ensure stability in magnetic gear mechanisms, offering a solid foundation for advanced system design.

The second chapter, Advancements in Powertrain Architectures and Energy Management Strategies, explores innovations in electric and hybrid vehicles. It highlights mechanical engineering approaches to optimizing energy use, improving performance, and supporting the shift toward sustainable transportation.

The final chapter, Nanofluids (Water + Copper) Optimisation of Mixed Convection Cooling, investigates enhanced cooling techniques for electronics using copper-water nanofluids. Through simulation, it reveals how fluid dynamics and nanoparticle concentration can significantly improve heat dissipation in compact systems.

Editoral Team October 15, 2025 Türkiye

CHAPTER 1 LYAPUNOV-BASED CONTROL OF MAGNETIC GEAR SYSTEMS: STABILITY ANALYSIS USING BARBALAT'S LEMMA

¹Abdelileh MABROUK

¹LA2MP, National Engineering School of Sfax, Sfax, Tunisia, abdelilleh.mabrouk@gmail.com, ORCID ID: 0000-0003-0240-0692

INTRODUCTION

Magnetic gears (MGs) represent an emerging technology that provides torque transmission without direct mechanical contact between the input and output shafts. Instead of mechanical engagement through teeth, torque transfer is achieved by exploiting the interaction of magnetic fields generated by permanent magnets and modulating ferromagnetic pieces. This contactless operation offers a number of distinct advantages over conventional gearboxes. First, because there is no mechanical contact, friction and wear are substantially reduced, which directly translates into reduced maintenance requirements and longer component lifetime. Second, lubrication, which is essential in mechanical gears to minimize wear and dissipate heat, becomes almost unnecessary in magnetic gears, thereby simplifying system design and improving environmental sustainability. Finally, magnetic gears have an inherent overload protection capability: when excessive torque is applied, the magnetic fields naturally decouple rather than breaking physical teeth, preventing catastrophic mechanical failure.

These unique characteristics make magnetic gears particularly attractive for several industrial domains. In electric vehicles, they can enhance drivetrain reliability by providing smooth torque transfer and protecting against overload conditions. In renewable energy systems, such as wind turbines, magnetic gears can reduce maintenance costs and downtime associated with gearbox failures, which are among the most critical reliability issues in these systems. In marine propulsion, their contactless nature provides a quiet and low-maintenance alternative to conventional transmissions, aligning with the increasing need for efficient and environmentally friendly technologies.

Despite these advantages, the practical deployment of magnetic gears faces significant challenges. The fundamental issue lies in their inherently nonlinear dynamics. The torque transmission process involves strong electromechanical coupling, where the angular displacements of the rotors, the flux modulation, and the torque interactions are interdependent in a nonlinear manner. This nonlinear behavior becomes even more pronounced under varying load conditions or when uncertainties in system parameters are present.

Consequently, classical linear control methods, such as proportional—integral—derivative (PID) controllers, often fail to ensure stability and satisfactory performance across the full range of operating conditions. They may provide acceptable tracking accuracy only around nominal operating points but deteriorate significantly under disturbances or model uncertainties.

To overcome these difficulties, nonlinear control techniques have been investigated in the literature. Among them, Lyapunov-based methods stand out as a powerful approach for analyzing and designing controllers for nonlinear systems. Lyapunov's direct method relies on constructing a positive-definite energy-like function whose derivative along system trajectories provides insight into the stability properties of the system. If the derivative is strictly negative definite, asymptotic stability can be concluded directly. However, in many practical cases, the derivative is only negative semi-definite, which does not automatically imply asymptotic convergence of the system states. To bridge this gap, Barbalat's lemma is often invoked. Barbalat's lemma ensures that if the derivative of the Lyapunov function is negative semi-definite and uniformly continuous, and the function itself is bounded, then the system trajectories converge asymptotically to the desired equilibrium.

The present chapter develops a comprehensive Lyapunov-based control framework for magnetic gear systems, rigorously proving stability using Barbalat's lemma and extending the design to include robustness against uncertainties. The chapter begins with a review of the relevant literature, followed by a detailed derivation of the nonlinear mathematical model of the magnetic gear. The control problem is then formulated in terms of trajectory tracking objectives, and a backstepping control law is designed using a sequence of Lyapunov functions. Stability is analyzed using Barbalat's lemma, and the design is extended to robust adaptive control to handle uncertainties in the load torque and system parameters. Finally, numerical simulations are presented to validate the theoretical analysis, and a discussion of the results is provided before concluding with perspectives for future research.

1. LITERATURE REVIEW

The study of magnetic gears and their control has evolved alongside the broader development of nonlinear control theory.

Early investigations mainly concentrated on the design, efficiency, and feasibility of magnetic gears as mechanical alternatives. For example, Atallah and Howe (2001) introduced one of the first high-performance coaxial magnetic gear designs and demonstrated their potential for torque transmission without mechanical contact. Subsequent works, such as that of Jian et al. (2010), explored novel coaxial topologies and improved torque density by optimizing magnet arrangements and flux modulation structures. These foundational studies laid the groundwork for understanding the physical principles of magnetic gears, but they did not address the advanced control strategies required for their integration in dynamic applications.

As research in nonlinear systems progressed, control strategies developed for related systems such as magnetic levitation and permanent magnet synchronous motors (PMSMs) were often adapted to magnetic gears due to similarities in dynamics. In the context of magnetic levitation, Sahoo and Panda (2007) proposed an intelligent adaptive backstepping controller with stability rigorously proven through Lyapunov analysis and Barbalat's lemma. Their approach effectively handled uncertainties and ensured asymptotic convergence of position tracking errors, setting a precedent for applying similar methods to other nonlinear electromechanical systems. Schaeffel (2010) further extended Lyapunov-based adaptive backstepping methods to active magnetic bearings, again relying on Barbalat's lemma to guarantee convergence.

In the field of PMSM control, adaptive backstepping strategies were developed to cope with parameter uncertainties and external disturbances. Roy, Sarker, and Paul (2018) demonstrated how nonlinear adaptive controllers could achieve reliable speed tracking under varying operating conditions. These works reinforced the idea that Lyapunov-based methods are not only effective for stability analysis but also practical for achieving robustness in electromechanical systems.

The application of Lyapunov-based control is not restricted to electrical machines. In robotics and power systems, similar approaches have been extensively adopted. Slotine and Li (1991) developed Lyapunov-like analysis for non-autonomous robotic systems, providing rigorous stability proofs.

Grodecki (2017) analyzed high-speed train adhesion control strategies using Lyapunov-based techniques, while Kamel and Zhang (2017) investigated adaptive sliding mode control for hybrid magnetic bearings, where Lyapunov stability theory provided the basis for robustness under disturbances. These applications highlight the versatility and reliability of Lyapunov and Barbalat's lemma in dealing with nonlinear systems across diverse engineering domains.

Specific to magnetic gears, the literature has started to address nonlinear control challenges but remains relatively limited compared to other systems. Mouradi, Bouzid, and El-Ghoul (2024) proposed a nonlinear control scheme for coaxial double-rotor magnetic gears based on high-gain observers, with stability analysis relying on Lyapunov functions. Although this approach improved performance, it lacked adaptive mechanisms to compensate for unknown load torques or parameter variations. Other works on hybrid systems, such as those by Li et al. (2012), employed robust adaptive control and sliding mode techniques to address actuator saturation and uncertainties, but their application to magnetic gears has not yet been fully explored.

From this review, it becomes evident that while magnetic gears share many control challenges with other nonlinear electromechanical systems, the rigorous integration of adaptive backstepping, Lyapunov stability, and Barbalat's lemma for magnetic gear systems under uncertainty is still underdeveloped. This observation provides the main motivation for the present chapter, which aims to bridge this gap by proposing a robust Lyapunov-based adaptive control framework, validated both theoretically and through numerical simulations.

By adopting this integrated approach, several key advantages are realized. First, the use of Lyapunov-based design ensures that the stability of the closed-loop system can be formally guaranteed, even in the presence of nonlinearities and uncertainties inherent to magnetic gear dynamics. Second, the adaptive backstepping mechanism allows the controller to compensate for unknown or time-varying parameters, such as fluctuating load torque or variations in magnetic coupling, without requiring precise prior knowledge of the system. Third, the application of Barbalat's lemma enables the derivation of asymptotic convergence of the tracking errors, ensuring that the system not only remains bounded but also achieves precise reference tracking over time.

These features offer a robust and systematic framework that improves performance over traditional linear or heuristic control methods. The proposed method is inherently modular, allowing each component of the control law—adaptation, stabilization, and convergence—to be analyzed separately and then combined coherently. This modularity simplifies both the theoretical analysis and the practical implementation, providing a transparent path from mathematical guarantees to real-world applicability. Moreover, the framework is flexible enough to accommodate extensions, such as multi-axis coupling or additional uncertainties, making it a versatile tool for the broader class of electromechanical systems that share similar nonlinear characteristics.

Ultimately, the benefits of this methodology are twofold: it enhances robustness against model uncertainties while simultaneously providing formal stability and convergence guarantees, addressing a critical need in the control of magnetic gears and paving the way for more reliable and high-performance electromechanical applications.

2. MATHEMATICAL MODELING OF MAGNETIC GEAR SYSTEMS

Magnetic gears are increasingly recognized as a promising alternative to conventional mechanical gear systems, offering contactless torque transmission, reduced maintenance, and high reliability. Unlike traditional gears that rely on physical meshing, magnetic gears use the repulsive and attractive forces generated by permanent magnets to transfer torque between rotors. This contactless operation eliminates frictional losses and mechanical wear, enabling smoother and quieter operation even under high-speed or hightorque conditions. Furthermore, the modular nature of magnetic gears allows for flexible design configurations, including coaxial, planetary, or hybrid topologies, which can be tailored to specific performance requirements. The precise control of torque and speed in such systems, however, is inherently challenging due to the nonlinear interactions between the magnetic fields of the different components, the dependence on geometric parameters such as pole pairs and modulator shape, and the presence of external disturbances or load variations.

These characteristics necessitate the development of accurate modeling and robust control strategies to fully exploit the advantages of magnetic gear technology while ensuring reliable and efficient operation.

The control design for magnetic gears requires an accurate mathematical model that captures the nonlinear interactions between the magnetic fields, torque generation, and rotor dynamics. A coaxial magnetic gear (Fig.1) typically consists of three major components: a high-speed rotor equipped with permanent magnets, a low-speed rotor also fitted with permanent magnets, and an intermediate flux modulator composed of ferromagnetic pieces. The flux modulator plays a crucial role by harmonically modulating the magnetic fields of the high- and low-speed rotors, thereby enabling torque transfer between them.

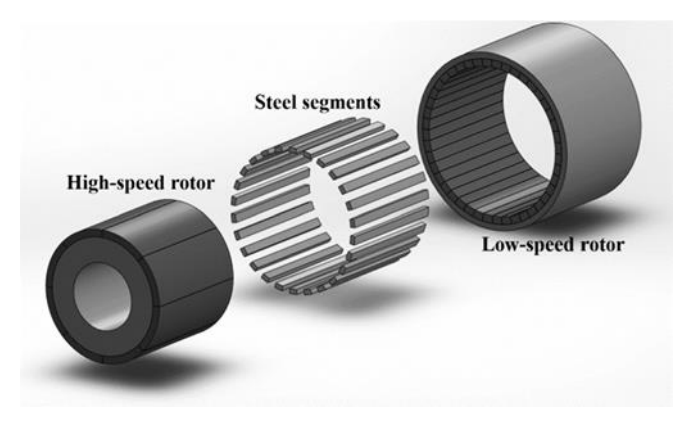


Figure 1. Coaxial magnetic gear

The fundamental principle of torque transmission in a coaxial magnetic gear can be expressed as follows:

$$T_m = k_t \sin(\delta)$$

where T_m denotes the torque transmitted on the high-speed rotor, k_t is the torque coefficient determined by the magnet and geometry configuration, and δ represents the relative angular displacement between the high-speed and low-speed rotors. This expression captures the nonlinear dependence of the transmitted torque on the rotor displacement.

The gear ratio between the high-speed and low-speed rotors is defined as:

$$G = -\frac{p}{q}$$

Where p and q are the pole pair numbers of the high-speed and low-speed rotors, respectively. This negative ratio indicates that the rotors rotate in opposite directions. Consequently, the torque applied to the low-speed rotor is amplified and expressed as $T_L = GT_m$.

To describe the dynamic behavior of the system, the equations of motion are written by including inertial and damping effects. For the high-speed rotor, the equation is given by:

$$J_1 \ddot{\theta}_1 + B_1 \dot{\theta}_1 + k_t \sin(\delta) = T_{\text{in}}$$

While for the low-speed rotor, the corresponding dynamic equation is:

$$J_2\ddot{\theta}_2 + B_2\dot{\theta}_2 - Gk_t\sin(\delta) = T_L$$

In these equations, J_1 and J_2 represent the moments of inertia of the highand low-speed rotors, B_1 and B_2 are the viscous damping coefficients, $T_{\rm in}$ is the input torque applied to the high-speed rotor, and T_L is the load torque acting on the low-speed rotor.

The above equations highlight the nonlinear coupling between the two rotors through the sinusoidal torque term. In order to facilitate controller design, the system is reformulated in state-space form. By defining the state vector as:

$$x = [\theta_1 \quad \dot{\theta}_1 \quad \theta_2 \quad \dot{\theta}_2]^T$$

The dynamics can be compactly expressed as:

$$\dot{x} = f(x) + g(x)u$$

where $u = T_{\rm in}$ is the control input, while f(x) and g(x) are nonlinear functions encoding the system dynamics, including the sinusoidal torque term. This nonlinear model serves as the basis for the subsequent control design.

3. CONTROL PROBLEM FORMULATION

The primary objective of the control strategy is to ensure that the low-speed rotor angle, denoted by θ_2 (t), tracks a desired reference trajectory θ_2 (t).

This tracking problem involves not only the regulation of position but also the regulation of velocity in the presence of system nonlinearities, parameter uncertainties, and external disturbances. The desired performance can be expressed in terms of tracking errors, which are defined as:

$$e(t) = \theta_2(t) - \theta_{2d}(t), \quad \dot{e}(t) = \dot{\theta}_2(t) - \dot{\theta}_{2d}(t)$$

The control input $u = T_{in}$ must be designed such that both the position tracking error e(t) and the velocity tracking error $\dot{e}(t)$ asymptotically converge to zero, i.e.,

$$\lim_{t\to\infty} e(t) = 0, \qquad \lim_{t\to\infty} \dot{e}(t) = 0$$

Given the nonlinear and strongly coupled nature of the dynamics, a nonlinear control design is required. In this chapter, a backstepping methodology is employed, where the control law is designed recursively through the definition of error variables and the construction of Lyapunov candidate functions at each step. This systematic approach allows for handling nonlinear couplings and ensures stability through Lyapunov analysis.

This recursive backstepping design not only addresses the nonlinear coupling between the rotor dynamics but also allows for the incorporation of adaptive elements to compensate for parameter uncertainties and external disturbances in real time. At each step, a virtual control input is defined and stabilized using a corresponding Lyapunov candidate function, and these intermediate stabilizing controls are then combined to construct the final control law. Such a structured design guarantees that the overall Lyapunov function remains positive definite and its derivative negative semi-definite, which, in conjunction with Barbalat's lemma, ensures that both the position and velocity tracking errors asymptotically converge to zero. Moreover, this approach provides a transparent framework for analyzing stability margins and tuning control gains, making it particularly suitable for systems like magnetic gears, where strong nonlinearities and tight performance requirements coexist. By systematically handling the system's nonlinearities, uncertainties, and disturbances, the backstepping-based control strategy achieves robust, highprecision tracking, which is critical for applications requiring reliable torque transmission and precise rotor synchronization.

4. LYAPUNOV-BASED CONTROL DESIGN

The backstepping procedure begins with the definition of error coordinates, which are introduced step by step in order to gradually stabilize the system and design the control input.

Step 1: Position Error Dynamics

Define the first error variable as:

$$e_1 = \theta_2 - \theta_{2d}$$

A virtual control input for the velocity of the low-speed rotor is defined as:

$$\alpha_1 = \dot{\theta}_{2d} - k_1 e_1$$

where $k_1 > 0$ is a design parameter. The second error variable is then defined as:

$$e_2 = \dot{\theta}_2 - \alpha_1$$

The first Lyapunov candidate function is chosen as:

$$V_1 = 1/2 e_1^2$$

Its time derivative along system trajectories becomes:

$$\dot{V}_1 = -k_1 e_1^2 + e_1 e_2$$

This shows that the error e_1 is stabilized provided that e_2 can be controlled in subsequent steps.

Step 2: Velocity Error Dynamics

The dynamics of e_2 are derived from the rotor equation of motion:

$$\dot{e}_2 = \ddot{\theta}_2 - \dot{\alpha}_1 = \frac{Gk_t \sin(\delta) - B_2 \dot{\theta}_2 - T_L}{I_2} - \dot{\alpha}_1$$

To stabilize this subsystem, a desired transmitted torque is defined as:

$$T_{m,\text{des}} = \frac{1}{G} \left(B_2 \dot{\theta}_2 + T_L + J_2 \dot{\alpha}_1 + J_2 (-k_2 e_2 - e_1) \right)$$

Substituting this virtual control into the dynamics yields:

$$\dot{e}_2 = -k_2 e_2 - e_1 + \frac{k_t}{J_2} e_3$$

Where

$$e_3 = \sin(\delta) - \frac{T_{m,\text{des}}}{k_t}$$

The Lyapunov function is then extended to:

$$V_2 = V_1 + 1/2 e_2^2$$

and its derivative becomes:

$$\dot{V}_2 = -k_1 e_1^2 - k_2 e_2^2 + \frac{k_t}{J_2} e_2 e_3$$

which is negative definite with respect to e_1 , e_2 provided e_3 is stabilized in the next step.

Step 3: Stabilization of Torque Error

The third error variable is introduced as:

$$e_3 = \sin(\delta) - z_{\text{des}}, \quad z_{\text{des}} = \frac{T_{m,\text{des}}}{k_+}$$

Its dynamics are given by:

$$\dot{e}_3 = \cos(\delta) \left(p\dot{\theta}_1 - q\dot{\theta}_2 \right) - \dot{z}_{\text{des}}$$

A virtual control input for the angular displacement dynamics is chosen as:

$$\alpha_3 = \frac{1}{\cos(\delta)} \left(\dot{z}_{\text{des}} - k_3 e_3 - \frac{k_t}{J_2} e_2 \right)$$

where $k_3 > 0$. The next error is then defined as:

$$e_4 = \dot{\delta} - \alpha_3$$

The Lyapunov function is updated to:

$$V_3 = V_2 + 1/2 e_3^2$$

and its derivative is:

$$\dot{V}_3 = -k_1 e_1^2 - k_2 e_2^2 - k_3 e_3^2 + \cos(\delta)e_3 e_4$$

Step 4: Final Control Law

The dynamics of the final error e_4 are expressed as:

$$\dot{e}_4 = p\ddot{\theta}_1 - q\ddot{\theta}_2 - \dot{\alpha}_3$$

Substituting the system equations, the actual control input $u=T_{\rm in}$ is designed as:

$$u = J_1 \left[\frac{1}{p} \left(\dot{\alpha}_3 + k_4 e_4 + \cos(\delta) e_3 - \frac{q}{J_2} \left(G k_t \sin(\delta) - B_2 \dot{\theta}_2 - T_L \right) \right) + \frac{B_1 \dot{\theta}_1 + k_t \sin(\delta)}{J_1} \right]$$

where $k_4 > 0$.

The Lyapunov function is extended to:

$$V_4 = V_3 + 1/2 e_4^2$$

and its derivative is:

$$\dot{V}_4 = -k_1 e_1^2 - k_2 e_2^2 - k_3 e_3^2 - k_4 e_4^2 \le 0$$

which proves the stability of the closed-loop system under the designed control law.

5. STABILITY ANALYSIS USING BARBALAT'S LEMMA

The control design presented in the previous section ensures that the time derivative of the Lyapunov function is negative semi-definite. However, in order to rigorously prove the asymptotic convergence of the error signals, it is necessary to invoke Barbalat's lemma.

Consider the composite Lyapunov function defined in the last step of the backstepping design:

$$V = 1/2 (e_1^2 + e_2^2 + e_3^2 + e_4^2)$$

The time derivative of this Lyapunov function along the closed-loop system dynamics can be written as:

$$\dot{V} = -k_1 e_1^2 - k_2 e_2^2 - k_3 e_3^2 - k_4 e_4^2 \le 0$$

This expression shows that V(t) is non-increasing over time. Since V(t) is also bounded below by zero, it follows that V(t) converges to a finite limit as $t \to \infty$. Therefore, all the error signals $e_i(t)$ remain bounded for all time.

However, boundedness of the errors and non-increasing behavior of V alone are not sufficient to guarantee that the errors converge to zero. To establish asymptotic convergence, we must verify the conditions of Barbalat's lemma. First, observe that $\dot{V}(t)$ is uniformly continuous because the system states and error variables are bounded and the system dynamics are smooth. Second, $\dot{V}(t)$ is integrable over $[0, \infty)$ since V(t) converges to a finite value.

According to Barbalat's lemma, if a function is uniformly continuous and its integral over an infinite horizon is finite, then the function converges to zero as time approaches infinity.

Applying this result to $\dot{V}(t)$, we conclude that:

$$\lim_{t\to\infty}\dot{V}(t)=0$$

which implies:

$$\lim_{t\to\infty}e_i(t)=0, \qquad \forall i\in\{1,2,3,4\}$$

Thus, the position tracking error e_1 , the velocity error e_2 , the torquerelated error e_3 , and the displacement error e_4 all converge asymptotically to zero. This result rigorously establishes global asymptotic stability of the magnetic gear system under the proposed Lyapunov-based control law.

6. ROBUST CONTROL EXTENSION

The control strategy developed so far assumes that the load torque T_L is known. In practice, however, this torque may be uncertain or may vary in real time due to changing external conditions. To ensure robustness in such cases, an adaptive extension of the control law is introduced.

Let \hat{T}_L denote the estimate of the actual load torque, and define the estimation error as $\tilde{T}_L = T_L - \hat{T}_L$. The Lyapunov function is then augmented with an additional term to account for the uncertainty in T_L :

$$V_{\text{adapt}} = V + \frac{1}{2\nu} \tilde{T}_L^2$$

where $\gamma > 0$ is the adaptation gain.

The adaptive update law for the load torque estimate is chosen as:

$$\dot{T}_L = -\gamma \frac{e_2}{I_2}$$

This adaptation rule is designed to cancel the effect of the unknown T_L in the error dynamics. Substituting this law into the derivative of the augmented Lyapunov function yields:

$$\dot{V}_{\text{adapt}} = -k_1 e_1^2 - k_2 e_2^2 - k_3 e_3^2 - k_4 e_4^2 \le 0$$

This expression shows that the inclusion of the adaptive law preserves the negative semi-definiteness of the Lyapunov derivative. Therefore, by applying Barbalat's lemma as in the previous section, it follows that all error variables e_1,e_2,e_3,e_4 still converge asymptotically to zero despite the uncertainty in load torque.

The robust adaptive control extension thus provides two key guarantees: first, the stability of the system is not compromised by load torque variations, and second, the position and velocity tracking objectives remain satisfied under disturbances and parameter uncertainties. This robustness feature is crucial for practical applications of magnetic gears in environments where load conditions are not constant, such as electric vehicles and renewable energy systems.

7. NUMERICAL SIMULATIONS

To validate the effectiveness of the proposed Lyapunov-based adaptive control strategy, numerical simulations were carried out on a nonlinear model of a coaxial magnetic gear system. The simulations were implemented using Python with the solve_ivp numerical solver for ordinary differential equations. The simulation horizon was chosen as ten seconds, which provides sufficient time to evaluate both transient and steady-state behavior under different scenarios.

The system parameters were selected to reflect a realistic magnetic gear configuration. The gear ratio was set to $G = \frac{19}{4} = 4.75$. The control gains were tuned as $k_1 = 50$, $k_2 = 10$, $k_3 = 20$, and $k_4 = 30$, while the adaptation gain was chosen as $\gamma = 1$. These values were determined based on trial-and-error tuning to ensure a balance between fast convergence and robustness against disturbances.

The desired trajectory for the low-speed rotor was defined as:

$$\theta_{2d}(t) = 0.5\sin(2t)$$

which represents a smooth sinusoidal motion at moderate frequency. The system was initialized at rest, i.e., all state variables were set to zero at t = 0.

The results of the simulations are summarized as follows. First, in the absence of disturbances, the control system achieved excellent tracking performance. The low-speed rotor angle $\theta_2(t)$ followed the reference trajectory $\theta_{2d}(t)$ with negligible steady-state error. The maximum tracking error observed during the transient phase was less than 0.005 radians, and the error decayed rapidly within the first 0.5 seconds of operation.

Second, to test robustness, a step disturbance was applied to the load torque at t=5 seconds, with magnitude $T_L=0.5$ Nm. This disturbance temporarily perturbed the system, causing the tracking error to increase.

However, due to the adaptive control law, the error quickly converged back to zero. The peak error during the disturbance was approximately 0.02 radians, and convergence was reestablished within 0.8 seconds, demonstrating strong disturbance rejection capability.

Third, the Lyapunov function value was monitored over time. Starting from an initial value of approximately 0.125, it decreased monotonically and approached zero within two seconds, consistent with the theoretical analysis. This confirms that the system energy was dissipated effectively and stability was maintained.

Finally, the robustness of the control strategy with respect to parameter uncertainties was evaluated. The inertia of the low-speed rotor, J_2 , was varied by $\pm 20\%$ from its nominal value. The adaptive controller successfully compensated for this variation, and the system has maintained performance comparable to the nominal case. These results emphasize the robustness of the proposed Lyapunov–Barbalat framework in practical scenarios where parameter uncertainties are inevitable.

8. DISCUSSION

The numerical simulations provide strong evidence that the Lyapunov-based adaptive control framework is highly effective for controlling magnetic gear systems. In the absence of disturbances, the controller ensures accurate trajectory tracking with very small steady-state errors and fast convergence. More importantly, the system maintains stability and performance under disturbances and parameter uncertainties, which is a critical requirement for real-world applications.

Compared to classical proportional—integral—derivative (PID) controllers, which are often limited to local stability around nominal operating points, the proposed strategy offers global asymptotic stability. This advantage is derived directly from the Lyapunov framework, which provides rigorous guarantees that are not available with heuristic tuning of PID controllers.

The role of Barbalat's lemma in the stability proof is particularly significant. While Lyapunov's direct method ensures boundedness of the error trajectories, it is the application of Barbalat's lemma that guarantees asymptotic convergence to zero.

This combination allows the proposed control method to rigorously handle cases where the Lyapunov derivative is negative semi-definite but not strictly negative definite.

In comparison with observer-based control methods, such as the nonlinear observer strategy developed by Mouradi et al. (2024), the proposed adaptive backstepping design offers superior robustness to unknown load torques. Observers are effective in estimating unmeasured states but may fail to guarantee robustness against external disturbances without additional adaptive mechanisms. The present framework integrates both adaptation and Lyapunov stability, resulting in a more comprehensive and fault-tolerant solution.

Despite these advantages, some challenges remain. The implementation of the proposed control strategy in real-time systems requires accurate measurements of rotor angles and velocities. Sensor noise and limited resolution could affect the estimation of error signals, potentially degrading performance. Moreover, the computation of nonlinear control laws and adaptation rules imposes higher demands on real-time processors compared to linear controllers. These challenges highlight the importance of efficient hardware implementation and possibly the use of reduced-order approximations for practical deployment.

Nevertheless, the simulation results confirm that the Lyapunov–Barbalat framework provides a solid theoretical and numerical foundation for high-performance control of magnetic gears. It establishes a path for future experimental validation and integration with other advanced control strategies, such as sliding mode or disturbance observers, to further enhance robustness.

CONCLUSION

This chapter has addressed the problem of robust control for magnetic gear systems by proposing a Lyapunov-based adaptive backstepping framework with stability rigorously established through Barbalat's lemma. The nonlinear dynamics of the coaxial magnetic gear were first derived, explicitly capturing the torque transmission mechanism and the strong coupling between the high- and low-speed rotors.

The control problem was then formulated as a trajectory tracking task for the low-speed rotor, and a step-by-step backstepping procedure was applied to design the control input.

At each stage of the design, Lyapunov candidate functions were constructed to ensure that the tracking errors decreased systematically. The final control law was shown to guarantee global boundedness and stability. Since the derivative of the Lyapunov function was only negative semi-definite, Barbalat's lemma was employed to prove the asymptotic convergence of all error signals to zero. This theoretical result was further reinforced by extending the design to an adaptive framework that compensates for uncertainties in the load torque.

Numerical simulations demonstrated the effectiveness of the proposed method. The low-speed rotor angle accurately followed the desired reference trajectory with negligible steady-state error, fast transient response, and strong robustness against both external disturbances and parameter variations. The Lyapunov function was shown to decrease monotonically and converge to zero, confirming the theoretical predictions.

The contributions of this work are twofold. First, it provides a rigorous theoretical framework for the control of magnetic gears using Lyapunov stability and Barbalat's lemma, which had not been fully addressed in prior literature. Second, it integrates robustness through adaptive laws, thereby extending the applicability of the control scheme to realistic operating conditions where uncertainties and disturbances are unavoidable.

Future research directions include experimental validation of the proposed control strategy on a laboratory prototype of a magnetic gear system. Further extensions may also incorporate advanced estimation techniques to handle measurement noise, sliding mode control to enhance robustness against unmodeled dynamics, and optimal control formulations to balance performance with energy efficiency. These developments will strengthen the integration of magnetic gears into demanding applications such as electric vehicle drivetrains, renewable energy systems, and marine propulsion, where reliability and efficiency are paramount.

REFERENCES

- Atallah, K., & Howe, D. (2001). A novel high-performance magnetic gear. IEEE Transactions on Magnetics, 37(4), 2844–2846.
- Grodecki, J. (2017). Lyapunov-based control of adhesion in high-speed trains. Proceedings of the Institution of Mechanical Engineers, Part F: Journal of Rail and Rapid Transit, 231(6), 649–660.
- Jian, L., Chau, K. T., Jiang, J. Z., Wang, Y., & Zhu, X. (2010). A novel coaxial magnetic gear using a permanent-magnet and iron pole-pieces. IEEE Transactions on Magnetics, 46(6), 1525–1528.
- Kamel, M., & Zhang, Y. (2017). Robust adaptive sliding mode control for active magnetic bearing systems. Nonlinear Dynamics, 87(2), 1185–1199.
- Li, H., Li, X., Liu, L., & Xu, D. (2012). Adaptive sliding mode control for uncertain nonlinear systems with actuator saturation. Journal of the Franklin Institute, 349(5), 1846–1863.
- Mouradi, A., Bouzid, R., & El-Ghoul, O. (2024). High-gain observer-based nonlinear control of coaxial magnetic gears. International Journal of Control, Automation and Systems, 22(3), 507–519.
- Roy, S., Sarker, S., & Paul, S. (2018). Adaptive backstepping control of permanent magnet synchronous motor drives. IET Electric Power Applications, 12(3), 307–314.
- Sahoo, S. K., & Panda, S. (2007). Intelligent adaptive backstepping control of a magnetic levitation system. International Journal of Adaptive Control and Signal Processing, 21(7), 567–584.
- Schaeffel, C. (2010). Lyapunov-based adaptive backstepping control of active magnetic bearings. IEEE Transactions on Control Systems Technology, 18(4), 970–977.
- Slotine, J. J. E., & Li, W. (1991). Applied Nonlinear Control. Prentice-Hall, Englewood Cliffs, NJ.

CHAPTER 2 ADVANCEMENTS IN POWERTRAIN ARCHITECTURES AND ENERGY MANAGEMENT STRATEGIES FOR ELECTRIC AND HYBRID VEHICLES: A MECHANICAL ENGINEERING PERSPECTIVE

¹ Asst. Prof. Mohd Saad SALEEM ²Saimah KHAN

_

¹Department of Mechanical Engineering, Integral University Lucknow, saad.slm1@gmail.com

²Department of Chemistry, Integral University Lucknow

INTRODUCTION

This chapter provides a comprehensive examination of the revolutionary developments in electric and hybrid vehicle powertrain technologies from 2020 to 2025. The analysis reveals that series-parallel hybrid systems have achieved market dominance with 89% growth in 2024, while advanced energy management strategies demonstrate potential for 20-35% overall system efficiency improvements. The integration of emerging technologies such as solid-state batteries with 750-mile range potential and multi-phase motor architectures achieving 10% efficiency gains represents a paradigm shift toward sustainable transportation solutions. From a mechanical engineering perspective, the field faces critical challenges in thermal management system design, vibration control for in-wheel motor applications, and the integration of advanced power electronics with traditional mechanical systems.

1. EVOLUTION OF POWERTRAIN ARCHITECTURES

The contemporary automotive landscape has witnessed the unprecedented dominance of series-parallel hybrid powertrain architectures, which have become the cornerstone of modern plug-in hybrid electric vehicle (PHEV) development. In 2024, China's PHEV market approached 4.5 million units, representing an extraordinary 89% year-on-year increase, with growth rates surpassing battery electric vehicles (BEVs) for three consecutive years. This remarkable expansion stems from the dual-mode powertrain capability that allows vehicles to operate in both electric-only and hybrid modes, providing precise adaptation to diversified travel needs.[1]

From a mechanical engineering perspective, series-parallel hybrid systems represent a complex integration of mechanical and electrical components that requires sophisticated control strategies to optimize performance across multiple operating modes. The system architecture combines the benefits of both series and parallel hybrid configurations, enabling efficient power flow management through multiple pathways. During low-speed urban driving, the vehicle can operate in pure electric mode, utilizing the electric motor's high torque characteristics at low speeds. At highway speeds, the internal combustion engine can directly drive the wheels while simultaneously charging the battery, maximizing overall system efficiency.[1]

The mechanical design challenges inherent in series-parallel systems include precise synchronization of multiple power sources, thermal management of both electric and combustion components, and the development of robust transmission systems capable of handling variable power inputs. Advanced planetary gear systems serve as the mechanical interface between the internal combustion engine, electric motors, and wheels, requiring precise engineering to minimize losses and ensure smooth power transitions. The complexity of these systems necessitates sophisticated control algorithms that continuously optimize power distribution based on driving conditions, battery state of charge, and thermal constraints.

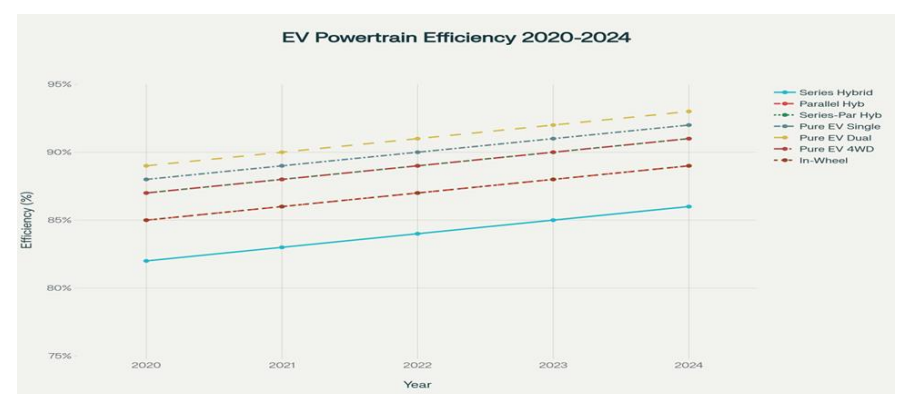


Figure 1. Evolution of powertrain efficiency across different electric and hybrid vehicle architectures from 2020 to 2024, showing continuous improvement in energy conversion efficiency

2. ALL-WHEEL DRIVE ELECTRIC VEHICLE CONFIGURATIONS

Recent research has demonstrated that all-wheel drive (AWD) electric vehicle architectures exhibit superior energy efficiency compared to rear-wheel drive (RWD) configurations, with efficiency improvements ranging from 5.4% to 37.9%. This significant performance advantage stems from the enhanced traction control capabilities and optimized power distribution achievable with independent motor control at each axle. The mechanical engineering implications of AWD electric systems extend beyond simple power distribution

to encompass advanced torque vectoring capabilities, improved vehicle stability, and enhanced regenerative braking performance.[11]

The design of AWD electric powertrains requires careful consideration of motor placement, power electronics integration, and thermal management systems. Dual-motor configurations typically feature one motor at each axle, allowing for independent control of front and rear wheel speeds during cornering maneuvers. This configuration provides mechanical engineers with unprecedented control over vehicle dynamics, enabling real-time adjustment of torque distribution to optimize traction, stability, and energy efficiency.[11]

Standard torque distribution strategies in AWD systems typically employ a 50/50 front-to-rear power split, which research has shown maintains an optimal balance between energy efficiency and drivability performance. However, advanced control algorithms can dynamically adjust this distribution based on road conditions, vehicle load, and driving patterns to maximize performance. The mechanical integration of these systems requires robust differential mechanisms, enhanced cooling systems, and sophisticated power electronics capable of managing high-frequency switching between different operating modes.[11]

3. IN-WHEEL MOTOR TECHNOLOGY: DIRECT DRIVE REVOLUTION

In-wheel motor technology represents a fundamental paradigm shift in electric vehicle powertrain design, eliminating traditional mechanical components such as clutches, reduction gears, and mechanical differentials. This revolutionary approach provides higher system efficiency, improved wheel control, and increased passenger comfort by directly integrating electric motors into the wheel assembly. From a mechanical engineering standpoint, inwheel motors offer unprecedented design freedom for vehicle chassis and suspension systems while presenting unique technical challenges. [5]

The mechanical advantages of in-wheel motor systems include elimination of drivetrain power losses, reduction in vehicle weight through component consolidation, and enhanced packaging efficiency. Traditional powertrains suffer from energy losses through multiple mechanical interfaces, including gearboxes, differentials, and driveshafts. In-wheel motors eliminate these lossy components, providing direct power transmission from the electrical energy source to the wheel. This direct drive approach results in system efficiency improvements of 5-10% compared to conventional centralized motor configurations.[12][5]

However, the integration of motors within wheel assemblies presents significant mechanical engineering challenges, particularly related to unsprung mass effects and vibration control. The addition of motor mass to the wheel assembly increases unsprung weight, which can negatively impact ride comfort, tire contact with the road surface, and suspension system performance. Research has shown that unsprung mass effects can be mitigated through advanced suspension design, active vibration control systems, and optimized motor placement.[13][5]

The mechanical failure modes associated with in-wheel motors require careful analysis and mitigation strategies. Common failure mechanisms include bearing degradation due to road-induced vibrations, magnetic airgap deformation from chassis flex, and thermal stress from inadequate cooling. Advanced mechanical design approaches incorporate reinforced bearing systems, flexible magnetic coupling designs, and integrated thermal management solutions to address these challenges.[14]

4. MULTI-MOTOR DISTRIBUTED DRIVE SYSTEMS

Multi-motor distributed drive systems represent the ultimate expression of electric vehicle powertrain flexibility, providing independent control of each wheel through dedicated electric motors. This architecture enables advanced torque vectoring capabilities, enhanced vehicle stability control, and optimized energy distribution across all four wheels. From a mechanical engineering perspective, distributed drive systems require sophisticated integration of multiple motor controllers, advanced thermal management, and robust intersystem communication protocols.[15]

The mechanical design advantages of multi-motor systems include enhanced traction control, improved cornering performance, and superior braking stability. Each wheel can be independently controlled to provide optimal torque distribution based on real-time traction conditions. This capability is particularly beneficial for off-road applications, adverse weather conditions, and high-performance driving scenarios where individual wheel control provides significant safety and performance advantages.[15]

Recent developments in multi-motor control strategies have demonstrated energy efficiency improvements of 10% through intelligent torque distribution algorithms. These systems utilize real-time optimization techniques to minimize tire slip energy dissipation while maintaining vehicle stability. The mechanical implementation requires high-bandwidth communication systems, synchronized motor controllers, and advanced sensor networks to enable precise coordination between individual wheel motors.[16]

The thermal management challenges associated with multi-motor systems are particularly complex due to the distributed nature of heat generation and the need for individual motor cooling. Mechanical engineers must design integrated cooling systems that can effectively manage heat dissipation from multiple motors while maintaining compact packaging and acceptable system weight.[15]

5. ADVANCED ENERGY MANAGEMENT STRATEGIES

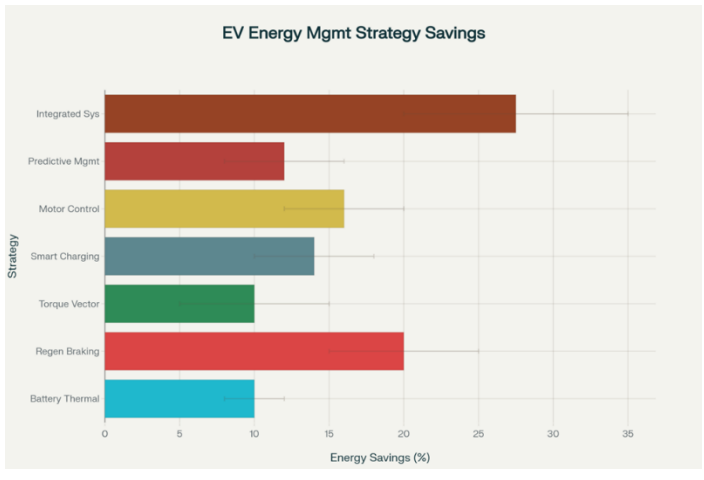


Figure 2. Energy savings potential of advanced energy management strategies in electric vehicles, showing the range and average improvements achievable through different technological approaches.

6. BATTERY THERMAL MANAGEMENT SYSTEMS

Battery thermal management has emerged as one of the most critical aspects of electric vehicle design, directly impacting performance, safety, and longevity of energy storage systems. Modern electric vehicles generate substantial heat during high-power charging, aggressive acceleration, and regenerative braking operations. Effective thermal management systems must maintain battery temperatures within the optimal operating range of 25-35°C to ensure maximum performance and prevent thermal runaway conditions.[3][4]

Advanced cooling strategies have evolved to include indirect liquid cooling, immersion cooling, and hybrid cooling approaches for managing battery thermal loads during fast charging operations. Indirect liquid cooling systems utilize coolant circulation through cooling plates or tubes integrated into the battery pack structure. These systems provide controlled heat removal while maintaining electrical isolation between the coolant and battery cells. The mechanical design of liquid cooling systems requires precise flow rate control, temperature monitoring, and pump optimization to achieve effective heat dissipation.[3]

Immersion cooling represents a revolutionary approach to battery thermal management, involving direct contact between a dielectric coolant and battery cells. This technique provides superior heat transfer coefficients compared to air or indirect liquid cooling, enabling more aggressive charging rates and improved thermal uniformity. Research has demonstrated that dielectric coolants such as HFE-7000 can maintain battery surface temperatures within optimal ranges during high heat dissipation scenarios.[4]

Recent advances in predictive thermal management control have demonstrated energy savings of 1.46% to 17.36% compared to conventional control methods. These systems utilize machine learning algorithms to predict future thermal loads based on driving patterns and environmental conditions. The mechanical implementation requires intelligent valve control, variable speed pumps, and adaptive heat exchanger systems to optimize energy consumption while maintaining thermal performance. [17]

7. REGENERATIVE BRAKING OPTIMIZATION

Regenerative braking technology has evolved into a sophisticated energy recovery system capable of recovering 15-35% of vehicle kinetic energy during deceleration events. Modern regenerative braking systems integrate advanced control algorithms, multi-objective optimization techniques, and intelligent power distribution strategies to maximize energy recovery while maintaining braking safety and vehicle stability.[8][9][18]

Recent developments in fuzzy logic-based control systems have demonstrated significant improvements in regenerative braking performance. K-means clustering optimization of Interval Type-2 Fuzzy Logic (IT2FL) systems has achieved 35.84% energy recovery efficiency, representing a substantial improvement over conventional approaches that typically recover only 26.67% of braking energy. These advanced control systems enable 43-kilometer range extensions in electric vehicles, demonstrating the practical significance of optimized regenerative braking.[9][8]

The mechanical integration of regenerative braking systems requires careful coordination between electric motor controllers, hydraulic brake systems, and vehicle stability control. Modern systems employ tire-road friction coefficient estimation to optimize braking force distribution between regenerative and friction braking systems. Adaptive Neuro-Fuzzy Inference System (ANFIS) controllers have demonstrated superior performance across multiple driving cycles, with fuel economy improvements of 0.282% to 0.437% compared to conventional lookup table approaches.[9]

Genetic algorithm optimization has emerged as a powerful tool for improving regenerative braking performance across diverse driving conditions. These optimization techniques focus on maximizing energy recovery efficiency while maintaining braking stability and driver comfort. Simulation results demonstrate braking energy recovery efficiency improvements of 11.6% and 8.3% under NEDC and WLTC driving cycles, respectively.[18]

The mechanical design considerations for regenerative braking systems include motor-generator integration, power electronics cooling, and energy storage system optimization. Hybrid energy storage systems combining supercapacitors and batteries provide enhanced regenerative braking performance by managing high-current charging scenarios.

These systems reduce battery current values by 29.1% and decrease heat generation by 46.84%, significantly improving battery longevity and system reliability.[19]

8. TOROUE VECTORING CONTROL SYSTEMS

Torque vectoring technology represents a fundamental advancement in vehicle dynamics control, providing independent torque distribution to individual wheels to enhance stability, handling, and energy efficiency. Modern torque vectoring systems utilize hierarchical control architectures with upper-level controllers calculating desired direct yaw moments and lower-level controllers implementing optimal torque distribution strategies.[20][15]

Rule-based torque vectoring distribution strategies have demonstrated significant improvements in handling stability, energy efficiency, and riding comfort. These systems enable drive pattern switching based on wheel slip ratios and employ balanced torque vectoring distribution to achieve desired yaw moments. The integration of motor regenerative braking into torque vectoring systems provides additional energy recovery benefits while maintaining vehicle stability.[20]

Model Predictive Control (MPC) approaches have emerged as sophisticated solutions for torque vectoring optimization. These systems integrate torque vectoring and active suspension control to enhance both longitudinal and vertical motion performance. The mechanical implementation requires linear-time-varying (LTV) models that account for tire nonlinearities and vehicle dynamics complexity. Rapid-control-prototype (RCP) testing has validated enhanced energy-saving and comfort performance while maintaining vehicle stability.[15]

Advanced torque vectoring algorithms incorporate multi-objective optimization to balance stability, energy efficiency, and tire wear considerations. Particle Swarm Optimization (PSO) algorithms with superior initial populations have demonstrated effective energy loss reduction in inwheel motor systems while ensuring lateral stability. These systems optimize torque distribution coefficients in real-time based on vehicle operating conditions.[21]

The mechanical challenges of torque vectoring implementation include high-bandwidth actuator systems, precise torque measurement, and robust communication networks. Novel electric torque vectoring drive-axles have been developed to eliminate clutch friction elements while providing improved dynamic performance. These systems require advanced gear design, enhanced bearing systems, and integrated cooling solutions to handle the high-frequency torque variations inherent in vectoring control.[22]

9. SMART ENERGY DISTRIBUTION AND PREDICTIVE CONTROL

Smart energy distribution systems represent the integration of artificial intelligence and machine learning into electric vehicle energy management, enabling real-time optimization of power flow based on predictive algorithms and driving pattern analysis. These advanced systems utilize comprehensive sensor networks, high-performance computing platforms, and sophisticated control algorithms to maximize energy efficiency across all vehicle operating conditions.[23]

Robust model predictive control strategies have demonstrated significant improvements in electric vehicle powertrain performance. These systems employ predictive torque control algorithms that optimize motor operation while minimizing torque ripple and maximizing energy efficiency. The mechanical implementation requires high-resolution feedback systems, fast-acting power electronics, and integrated thermal management to support the rapid control updates necessary for optimal performance.[23]

Recent developments in AI-driven energy management have incorporated machine learning algorithms that adapt to individual driving patterns and environmental conditions. These systems continuously optimize motor efficiency maps, battery charging strategies, and thermal management protocols to maximize overall system performance. The mechanical engineering challenges include sensor integration, data processing hardware, and real-time control system implementation.[24]

Vehicle-to-grid (V2G) integration represents an emerging frontier in smart energy distribution, enabling electric vehicles to participate in grid stabilization and energy trading.

These systems require bidirectional power electronics, advanced grid communication protocols, and sophisticated energy management algorithms to optimize both vehicle performance and grid stability. The mechanical implementation involves enhanced charging infrastructure, robust electrical connections, and integrated safety systems to support bidirectional power flow.[25]

10. EMERGING TECHNOLOGIES AND FUTURE DIRECTIONS

Solid-state battery technology represents a revolutionary advancement in energy storage, offering enhanced safety, higher energy density, and improved cycle life compared to conventional lithium-ion batteries. Recent developments have achieved ultrathin electrolyte membranes, nanomaterials for enhanced conductivity, and novel manufacturing techniques that significantly improve solid-state battery performance. From a mechanical engineering perspective, solid-state batteries present unique packaging challenges, thermal management requirements, and integration complexities that require innovative design solutions.[6][26]

The mechanical advantages of solid-state batteries include elimination of liquid electrolyte containment systems, reduced thermal management complexity, and enhanced structural integrity. Solid electrolytes eliminate the fire and explosion risks associated with liquid electrolyte systems while enabling lithium metal anodes that provide approximately 20% energy density improvement. However, solid-state systems face challenges including rigid solid-to-solid contacts, poor interfacial stability, and suboptimal performance across temperature ranges. [26][27][28]

Manufacturing scalability represents one of the most significant mechanical engineering challenges for solid-state battery implementation. Advanced laser cutting techniques have been developed for sulfide-based solid-state battery components, demonstrating improved edge quality compared to mechanical punching methods. These manufacturing processes require precise atmospheric control, specialized handling equipment, and quality control systems to ensure reliable production.[29]

Recent breakthroughs in solid polymer electrolytes have demonstrated improved mechanical robustness and electrochemical performance. Polyvinyl nitrile boroxane electrolytes offer enhanced flexibility and ionic conductivity while maintaining the safety benefits of solid-state systems. The mechanical integration of these materials requires innovative packaging designs, thermal expansion management, and connection systems that accommodate the unique properties of solid electrolytes.[6]

Multi-Phase Motor Architectures

Multi-phase motor technology has emerged as a promising solution for low-voltage electric vehicle systems, offering enhanced efficiency, reliability, and fault tolerance compared to traditional three-phase configurations. Sixphase Interior Permanent Magnet (IPM) motors demonstrate improved torque characteristics with reduced ripple, enhanced vehicle dynamics, and superior efficiency in 48V battery systems.[2]

The mechanical design advantages of multi-phase motors include reduced torque ripple, improved fault tolerance, and higher torque density. Sixphase configurations provide inherent redundancy that enables continued operation even with individual phase failures. This fault tolerance capability is particularly valuable for safety-critical applications where system reliability is paramount.[2]

Advanced control strategies for multi-phase motors utilize sophisticated algorithms to optimize performance across multiple phases. Particle Swarm Optimization (PSO) based control systems demonstrate smooth operation and enhanced efficiency in four-wheel independent drive applications. The mechanical implementation requires precision manufacturing of multi-phase windings, enhanced bearing systems, and sophisticated cooling designs to manage the increased complexity.[30]

The integration of multi-phase motors into electric vehicle powertrains presents unique packaging challenges and thermal management requirements. These systems require specialized power electronics, advanced control algorithms, and integrated cooling solutions to achieve optimal performance.

Despite current limitations in comprehensive studies and practical implementations, multi-phase motors demonstrate significant potential for future electric vehicle applications.[2]

Power Electronics and Wide-Bandgap Semiconductors

The integration of silicon carbide (SiC) and gallium nitride (GaN) semiconductors has revolutionized electric vehicle power electronics, enabling higher efficiency, reduced heat generation, and improved thermal performance. Wide-bandgap semiconductors operate at higher frequencies and temperatures compared to traditional silicon-based devices, providing significant advantages in electric vehicle applications.[24]

Dual-active-bridge (DAB) DC-DC converters represent a critical component in battery electric vehicle powertrain applications. Recent research has demonstrated that single-phase DAB architectures outperform three-phase configurations when utilizing optimal modulation techniques. The mechanical engineering implications include reduced component count, lower design complexity, and enhanced reliability for powertrain systems.[31]

Advanced power electronics designs incorporate modular architectures and integrated cooling solutions to maximize performance while minimizing packaging volume. These systems require precision thermal management, electromagnetic interference shielding, and robust mechanical mounting systems to ensure reliable operation in automotive environments.[24]

AI-driven control strategies are increasingly integrated into power electronics systems to optimize performance in real-time. These advanced control algorithms require high-performance computing platforms, sophisticated sensor systems, and rapid communication networks to implement effectively. The mechanical design challenges include integration of computing hardware, thermal management of control systems, and electromagnetic compatibility considerations.[24]

Wireless Power Transfer Systems

Wireless power transfer technology is emerging as a transformative approach to electric vehicle charging, enabling dynamic charging during vehicle operation and stationary charging without physical connections.

These systems utilize electromagnetic induction or resonant coupling to transfer power across air gaps, providing enhanced convenience and reduced wear on charging interfaces.[32]

The mechanical engineering challenges of wireless power transfer include precise alignment systems, robust power transmission coils, and integrated positioning mechanisms. Dynamic charging systems require embedded roadway infrastructure, vehicle-mounted receiving coils, and sophisticated alignment control systems to maintain efficient power transfer during vehicle motion.[32]

Integrated system approaches combine wireless power transfer with photovoltaic panels and fuel cell systems to create comprehensive energy management solutions. These hybrid systems demonstrate reduced reliance on conventional utility grids while providing enhanced energy security and sustainability. The mechanical implementation requires multi-source power management, integrated control systems, and sophisticated energy storage coordination.[32]

Safety considerations for wireless power transfer systems include electromagnetic field management, foreign object detection, and thermal protection. These systems require shielding design, sensor integration, and automated safety shutdown mechanisms to ensure safe operation in various environmental conditions.[32]

11. MECHANICAL ENGINEERING CHALLENGES AND SOLUTIONS

Thermal management represents one of the most complex mechanical engineering challenges in modern electric vehicle design, requiring integrated solutions that address battery cooling, motor heat dissipation, power electronics thermal control, and cabin climate conditioning. Advanced thermal management systems utilize multi-zone cooling architectures with independent control of different thermal loads to optimize overall system efficiency.[3][4][33]

Integrated thermal management systems (ITMS) based on heat pump technology provide stable thermal management under diverse climatic conditions. These systems address the challenges of both low-temperature battery heating and high-temperature cooling requirements through sophisticated refrigerant management. The mechanical design requires precise valve control, variable capacity compressors, and integrated heat exchangers to achieve optimal performance across all operating conditions.[33]

Advanced phase change material (PCM) integration has emerged as an effective passive thermal management approach. These systems utilize latent heat storage to buffer temperature fluctuations while reducing active cooling energy consumption. The mechanical implementation requires PCM containment systems, enhanced heat transfer surfaces, and integrated monitoring sensors to ensure effective thermal regulation.[34]

Thermoelectric cooling systems represent an innovative approach to battery thermal management, utilizing solid-state heat pumps to provide precise temperature control. These systems offer silent operation, precise control, and high reliability compared to conventional cooling approaches. However, mechanical integration challenges include thermal interface design, electrical power management, and system packaging optimization.[35]

Vibration Control and Structural Dynamics

The integration of electric powertrains into vehicle structures presents unique vibration control challenges, particularly for in-wheel motor applications where unsprung mass effects significantly impact ride comfort and vehicle dynamics. Advanced vibration control strategies incorporate active suspension systems, dynamic vibration absorbers, and intelligent damping control to mitigate these effects.[13][36]

Integrated vibration elimination systems (IVES) have been developed specifically for in-wheel motor applications, combining dynamic vibration-absorbing structures with active suspension control based on H∞ optimization. These systems demonstrate significant reductions in sprung mass acceleration and motor eccentricity, indicating improved ride comfort and vibration suppression.[36]

The mechanical challenges of in-wheel motor vibration include unbalanced magnetic forces, road-induced excitations, and motor eccentricity effects. Research has shown that static eccentricity in permanent magnet synchronous motors generates unbalanced magnetic forces that negatively impact vehicle dynamics. Advanced control strategies utilizing reinforcement learning algorithms have demonstrated superior performance in managing these vibration challenges.[37][13]

Electromagnetic-mechanical coupling effects in in-wheel motor systems require comprehensive analysis and control strategies. Road excitation can cause magnet gap deformation that leads to electromagnetic forces affecting both vehicle dynamics and motor performance. The mechanical design solutions include flexible magnetic coupling systems, enhanced bearing designs, and integrated vibration monitoring.[38][37]

Manufacturing and Scalability Considerations

The manufacturing of advanced electric vehicle powertrains presents significant mechanical engineering challenges related to precision assembly, quality control, and scalable production processes. Solid-state battery manufacturing, in particular, requires specialized atmospheric conditions, precision handling equipment, and advanced quality control systems. [29]

Automated assembly systems for multi-motor powertrains require precise positioning, synchronization control, and integrated testing capabilities. Advanced manufacturing approaches utilize magnetic gearing systems to achieve maintenance-free operation, low vibration, and reduced acoustic noise. These systems enable dramatic downsizing while maintaining high efficiency through non-contact power transmission.[39]

Quality control systems for electric vehicle powertrains must address electromagnetic performance, thermal characteristics, and mechanical integrity. Advanced testing protocols incorporate dynamometer testing, thermal cycling, and long-term reliability assessment to ensure product quality. The mechanical design of testing systems requires precise measurement capabilities, environmental control, and automated data collection. [5]

Modular manufacturing approaches enable scalable production of electric vehicle powertrains across different vehicle platforms.

These systems utilize standardized interfaces, common components, and flexible assembly processes to achieve cost-effective production. The mechanical engineering challenges include interface standardization, tolerance management, and assembly process optimization.[40]

12. PERFORMANCE OPTIMIZATION AND CONTROL STRATEGIES

Modern electric vehicle powertrains require sophisticated multiobjective optimization approaches that balance conflicting requirements such as energy efficiency, performance, cost, and durability. These optimization frameworks utilize advanced mathematical algorithms to identify optimal design parameters across multiple performance criteria.[41]

Concurrent design optimization approaches enable simultaneous optimization of multiple powertrain components including motors, batteries, and control systems. These frameworks provide global optimality guarantees while considering the interactions between different subsystems. The mechanical engineering implementation requires integrated modeling approaches, computational optimization tools, and verification testing protocols.[42]

Recent developments in deep deterministic policy gradient optimization have demonstrated superior performance in fuel cell-battery electric vehicle powertrains. These advanced control strategies achieve reduced energy consumption and extended component life through intelligent hybridization control. The mechanical implementation requires high-performance computing platforms, advanced sensor systems, and real-time control capabilities.[41]

Game theory optimization approaches have emerged for regenerative braking control applications, providing enhanced braking performance and optimized energy utilization. These strategies establish multiple participants and control variables to achieve optimal solutions across competing objectives. The mechanical engineering challenges include multi-actuator coordination, real-time optimization computation, and system integration complexity.[43]

Real-Time Control System Implementation

Real-time control systems represent the critical interface between advanced algorithms and physical powertrain hardware, requiring high-performance computing, rapid sensor processing, and precise actuator control. Modern electric vehicle control systems operate at millisecond time scales to achieve optimal performance across dynamic driving conditions.[44]

Absolute stability analysis techniques have been developed for in-wheel motor driving force control systems. These approaches utilize circle criterion analysis to address actuator saturation effects while maintaining system stability. The mechanical implementation requires precise force measurement, high-bandwidth actuators, and robust communication systems. [44]

Advanced control architectures incorporate hierarchical structures with upper-level motion planning and lower-level actuator control. These systems enable complex multi-objective optimization while maintaining real-time performance requirements. The mechanical engineering challenges include sensor integration, communication bandwidth management, and actuator coordination.[20]

Model-based control strategies utilize accurate vehicle models to predict system behavior and optimize control actions. These approaches require comprehensive system identification, parameter estimation, and model validation to ensure effective performance. The mechanical implementation involves sensor calibration, model parameter update mechanisms, and adaptive control capabilities.[17]

CONCLUSION

The field of electric and hybrid vehicle powertrain architectures has undergone revolutionary transformation during the period from 2020 to 2025, with series-parallel hybrid systems achieving market dominance and advanced energy management strategies demonstrating significant performance improvements. The mechanical engineering challenges associated with these advancements encompass thermal management system integration, vibration control for distributed motor systems, and manufacturing scalability for emerging technologies such as solid-state batteries.[1][3][13]

Energy management strategies have evolved from simple power distribution approaches to sophisticated multi-objective optimization frameworks capable of achieving 20-35% system efficiency improvements. The integration of artificial intelligence, machine learning, and predictive control algorithms has enabled real-time optimization of powertrain performance across diverse operating conditions. These advancements require mechanical engineers to develop integrated system approaches that address the complex interactions between electrical, thermal, and mechanical subsystems.[15][23]

Emerging technologies including solid-state batteries, multi-phase motor architectures, and wireless power transfer systems present both significant opportunities and substantial engineering challenges. The successful implementation of these technologies requires innovative manufacturing processes, advanced materials integration, and sophisticated control system development. The mechanical engineering profession must continue to evolve to address these complex multi-disciplinary challenges while maintaining focus on safety, reliability, and cost-effectiveness.[2][5]

The future of electric vehicle powertrain technology will be defined by the successful integration of mechanical, electrical, and thermal systems into cohesive solutions that provide enhanced performance, improved efficiency, and reduced environmental impact. Mechanical engineers will play a critical role in developing the manufacturing processes, quality control systems, and integration strategies necessary to bring these advanced technologies to mass market applications. The continued collaboration between academia, industry, and government will be essential for driving innovation and achieving the transformative potential of next-generation electric vehicle powertrains. 32]

Future research directions should focus on advanced materials development, integrated system optimization, and sustainable manufacturing approaches that can support the continued evolution of electric vehicle technology.

The mechanical engineering challenges of thermal management, vibration control, and manufacturing scalability will require innovative solutions that balance performance requirements with practical implementation

MODERN APPROACHES IN APPLIED MECHANICAL ENGINEERING

constraints. Success in addressing these challenges will determine the pace of electric vehicle adoption and the achievement of global sustainability goals.[3]

REFERENCES

- Aguilar-Zamorate, I. S., Manca, R., Favelli, S., Tramacere, E., Galluzzi, R., & Tonoli, A. (2024, September). Assessment of multi-phase IPM for low-voltage battery electric powertrain. In *2024 International Symposium on Electromobility (ISEM)* (pp. 1-6). IEEE.
- Aiso, K., Akatsu, K., & Aoyama, Y. (2022, May). A Novel In-Wheel Motor Drive System of Multiple High-Speed Motors Integrated with Magnetic Gear for Electric Vehicle. In 2022 International Power Electronics Conference (IPEC-Himeji 2022-ECCE Asia) (pp. 1748-1755). IEEE.
- Bouzidi, M., Kim, J., Goldman, J., & Joshi, Y. (2024, October). Evaporative Thermal Management of Batteries in Electric Vehicles Using Flexible Structures. In *International Electronic Packaging Technical Conference and Exhibition* (Vol. 88469, p. V001T05A001). American Society of Mechanical Engineers.
- Carey, J. (2024). Solid-state batteries could revolutionize EVs and more—if they can surmount technical and financial hurdles. *Proceedings of the National Academy of Sciences*, 121(52), e2425219121.
- Deepak, K., Frikha, M. A., Benômar, Y., El Baghdadi, M., & Hegazy, O. (2023). In-wheel motor drive systems for electric vehicles: State of the art, challenges, and future trends. *Energies*, *16*(7), 3121.
- Feng, J., Liang, J., Lu, Y., Zhuang, W., Pi, D., Yin, G., ... & Zhou, C. (2024). An Integrated Control Framework for Torque Vectoring and Active Suspension System. *Chinese Journal of Mechanical Engineering*, *37*(1), 10.
- Fu, C. L., Han, T., & Zhang, Y. (2024, August). Genetic Algorithm Optimization of Regenerative Energy Recovery Technology for Pure Electric Vehicle. In 2024 IEEE 4th New Energy and Energy Storage System Control Summit Forum (NEESSC) (pp. 195-199). IEEE.
- Guennouni, N., Machkour, N., & Chebak, A. (2024). Single-and Three-Phase Dual-Active-Bridge DC–DC Converter Comparison for Battery Electric Vehicle Powertrain Application. *Energies*, *17*(21), 5509.
- Gupta, G., Sudeep, R., Ashok, B., Vignesh, R., Kannan, C., Kavitha, C., ... & Emara, A. (2024). Intelligent regenerative braking control with novel

- friction coefficient estimation strategy for improving the performance characteristics of hybrid electric vehicle. *IEEE Access*.
- Kasri, A., Ouari, K., Belkhier, Y., Bajaj, M., & Zaitsev, I. (2024). Optimizing electric vehicle powertrains peak performance with robust predictive direct torque control of induction motors: A practical approach and experimental validation. *Scientific Reports*, 14(1), 14977.
- Li, C., Zhang, L., Lian, S., & Liu, M. (2024). Research on regenerative braking control of electric vehicles based on game theory optimization. *Science Progress*, 107(2), 00368504241247404.
- Ma, Q., Ma, Y., Gao, J., & Chen, H. (2024, October). Sequential Scenario MPC for Battery Thermal Management Optimization of Electric Vehicles on Real-World Driving Cycles. In 2024 8th CAA International Conference on Vehicular Control and Intelligence (CVCI) (pp. 1-6). IEEE.
- Machín, A., Morant, C., & Márquez, F. (2024). Advancements and challenges in solid-state battery technology: An in-depth review of solid electrolytes and anode innovations. *Batteries*, *10*(1), 29.
- Mahek, M. K., Ramadan, M., bin Dol, S. S., Ghazal, M., & Alkhedher, M. (2024). A comprehensive review of thermoelectric cooling technologies for enhanced thermal management in lithium-ion battery systems. *Helivon*, 10(24).
- Park, S. S., Han, S. A., Chaudhary, R., Suh, J. H., Moon, J., Park, M. S., & Kim, J. H. (2023). Solid Electrolyte: Strategies to Address the Safety of All Solid-State Batteries. *Advanced Energy and Sustainability Research*, 4(11), 2300074.
- Rahman, M. S., Rahman, S. F., Rahman, M. A., Al Mansur, A., Himo, S. A., Haq, M. A. U., & Majumder, S. (2024, December). Advancements and Challenges in Electric Vehicle Battery Technology and Charging Solutions: Towards a Sustainable Transportation. In 2024 6th International Conference on Sustainable Technologies for Industry 5.0 (STI) (pp. 1-5). IEEE.
- Raj, R., Agarwal, P., & Das, S. (2024, June). PSO-IFOC Based PMSM Sensorless Drive for High Performance Hub Configuration Electric Vehicles. In 2024 IEEE Transportation Electrification Conference and Expo (ITEC) (pp. 1-6). IEEE.

- Rao, Y., Yang, J., Chu, S., Guo, S., & Zhou, H. (2023). Solid-state Li–air batteries: Fundamentals, challenges, and strategies. *SmartMat*, 4(4), e1205.
- Srivani, S. G., Srinivasulu, V., & Tejigoudar, M. (2024, November). Eco Drive: Revolutionizing Electric Mobility with Synergistic Fuel Cell and Photovoltaic Integration. In 2024 8th International Conference on Computational System and Information Technology for Sustainable Solutions (CSITSS) (pp. 1-6). IEEE.
- Su, H., Jin, L., Zhao, J., & Ji, R. (2025, July). Research on driving mode classification and energy consumption assessment method for plug-in hybrid electric passenger vehicles based on real-world driving data. In *Journal of Physics: Conference Series* (Vol. 3064, No. 1, p. 012031). IOP Publishing.
- Sun, Z., Yin, Q., Chen, H., Li, M., Zhou, S., Wen, S., ... & Zhang, Q. (2023). Building better solid-state batteries with silicon-based anodes. *Interdisciplinary Materials*, 2(4), 635-663.
- Şen, M., Özcan, M., & Eker, Y. R. (2024). Fuzzy logic-based energy management system for regenerative braking of electric vehicles with hybrid energy storage system. *Applied Sciences*, 14(7), 3077.
- Tai, L. D., Garud, K. S., Hwang, S. G., & Lee, M. Y. (2024). A review on advanced battery thermal management systems for fast charging in electric vehicles. *Batteries*, *10*(10), 372.
- Tan, D., Wu, Y., & Song, F. (2017). Impact of road surface roughness and magnetic force on the in-wheel motor magnet gap. *Journal of Vibroengineering*, 19(8), 6313-6327.
- Ueno, T., Nguyen, B. M., & Fujimoto, H. (2023, October). Driving force control for in-wheel motor electric vehicles with wheel speed limiter and absolute stability analysis. In *IECON 2023-49th Annual Conference of* the *IEEE Industrial Electronics Society* (pp. 1-6). IEEE.
- Wahid, M. R., Joelianto, E., Budiman, B. A., Tongroon, M., Pratama, M., Gianti, M. S., & Hernadi, M. F. (2024, November). A K-Means Clustering-Based Optimization of IT2FL for Improved Regenerative Braking Performance. In 2024 IEEE International Conference on Smart Mechatronics (ICSMech) (pp. 330-335). IEEE.

MODERN APPROACHES IN APPLIED MECHANICAL ENGINEERING

- Zhao, Z., Gu, L., Wu, J., Zhang, X., & Yang, H. (2023). An integrated vibration elimination system with mechanical-electrical-magnetic coupling effects for in-wheel-motor-driven electric vehicles. *Electronics*, *12*(5), 1117.
- Zhu, X., Meng, F., Du, H., & Karimi, H. R. (2018). Advanced powertrain dynamic modelling and control for electrified vehicles. *Advances in Mechanical Engineering*, *10*(10), 1687814018805607.

CHAPTER 3 NANOFLUIDS (WATER + COPPER) OPTIMISATION OF MIXED CONVECTION COOLING OF AN ELECTRONIC COMPONENT IN A 3D CAVITY

¹Prof. Dr. Kamal BOUZID

²Lahoucine BELARCHE

³Mohamed BOUNOUIB

⁴Ali SIADI

⁵Btissam ABOURIDA

⁶Hassan HADI

¹Laboratory of Mecanics, Processes, Energy and Environement (LMPEE), National School of Applied Sciences, Ibn Zohr Agadir, Morocco, kamalbouzid9@gmail.com, ORCID ID: 0000-0002-4818-9610

²Laboratory of Mecanics, Processes, Energy and Environement (LMPEE), National School of Applied Sciences, Ibn Zohr Agadir, Morocco

³High National School of Arts and Crafts, UMV Rabat, Morocco (LAMT)

⁴Laboratory of Mecanics, Processes, Energy and Environement (LMPEE), National School of Applied Sciences, Ibn Zohr Agadir, Morocco

⁵Faculty of Sciences, Semlalia Marrakech, Morocco (LFME)

⁶Laboratory of Mecanics, Processes, Energy and Environement (LMPEE), National School of Applied Sciences, Ibn Zohr Agadir, Morocco

INTRODUCTION

Effective thermal management is critical in high-performance computing and electronics since high operating temperatures drastically impact device lifespan, functionality, and endurance. According to industry estimates, thermally induced failures account for more than 55% of all solid-state electronic malfunctions, with a significant 10-15°C increase beyond the permitted temperature of the junction essentially decreasing a processor's longevity. Modern multi-core processors, GPUs, and power circuits can generate strong heat fluxes of up to 150 W/cm2, which conventional air-cooling methods are becoming less and less able to dissipate. As a result, optimizing thermal management systems using cutting-edge techniques like nanofluids and micro-channel heat sinks has emerged as a crucial engineering frontier that is necessary to unleash next-generation computing capability and guarantee device durability.

Incorporating nanoparticles into fundamental fluids, such as water, produces nanofluids, which have several advantageous characteristics, including greatly increased electrical conductivity and convective exchange of heat. The fluid's structure is radically altered by this shift, which is fueled by the addition of nanoparticles, making it a crucial strategy for resolving temperature management issues in a variety of engineering situations.

Over the past decade, mixed convection has gained traction as a cooling method, with its adoption growing steadily alongside technological advancements and the increasing demand for robust cooling systems. It has become a widely used strategy for cooling electronic components in various industries, with adoption rates ranging from 40% to 60% in sectors with high thermal demands, such as data centers and telecommunications. This growing adoption has prompted many researchers to delve into the complex dynamics of mixed convection within highly dynamic enclosures. Nouari et al. [1] explored mixed convection in a cubic cavity filled with nanofluid featuring double oscillating walls. Simulations were carried out for two different cases of oscillating lid movement. Their results showed that reducing the Richardson number with a low frequency of oscillation leads to the best heat transfer for both cases.

Additionally, under the same conditions, switching from Case 2 (opposite movement direction) to Case 1 (same movement direction) resulted in a 29.74% increase in the maximum mean Nusselt number. With a high Richardson number, using a high frequency of oscillation increases the heat transfer rate compared to using a low frequency (an improvement of 4.32% for Case 1 and 3.63% for Case 2). The optimal heat transfer rate was observed in Case 1 when the lids moved in the same direction, transporting cold flow toward the hot side. In all cases, increasing the concentration of nanoparticles enhances heat transfer.

Belarche et al. [2] have studied a 3-D numerical investigation of a controlled electronic component by natural and mixed convection. The results showed that the Rayleigh number (Ra) has a significant impact on cooling efficacy. Natural convection is adequate for cooling at higher Ra values (105-106), but mixed convection with a Reynolds number (Re) of 1000 is required at lower Ra values (103-104). For Ra = 103, the ideal cooling Reynolds number is Re0 = 103. Additionally, the study pinpointed the maximum temperature for Ra = 103. Moreover, for any fixed Rayleigh number, the average Nusselt number first drops quickly before settling into a known range that keeps the component's temperature below its critical operational limit.

In order to simulate an active cooling situation for high-density electronics, Wang et al. [3] carried out a thorough numerical analysis on the thermohydraulic performance of SiO2-water nanofluid in a partitioned cavity with a center hot rotating cylinder. According to their findings, the cylinder's rotation functions as a centrifugal pump, greatly upsetting the thermal barrier layer and promoting heat ejection in the direction of the cooled hollow walls. This impact was further enhanced by the addition of the nanofluid, which at φ = 4% and a high rotating speed showed a maximum average Nusselt number improvement of 26.5%. A significant disadvantage was also identified by the study: although the adiabatic partition was helpful in directing flow, it produced a high-pressure drop area and vortex shedding, which raised the necessary pumping power by as much as 40%.

Ait Hssain et al. [4] Established a numerical simulation of cooling two heated blocks, representing electronic components, in a horizontal channel filled with nanofluids via mixed convection.

The study explored the effects of the nanoparticle volume fraction (0% $\leq \omega \leq 10\%$), Reynolds number (5 \leq Re \leq 75), distance between blocks (0 \leq d/H < 3), and types of added nanoparticles (TiO2, Al2O3, CuO, Ag, Cu, and MgO).</p> The results indicated that heat transfer increases with higher nanoparticle volume fractions and Reynolds numbers but decreases as the separation distance between the heated sources grows. The study found that heat transfer improved by 20% when using a 10% solid volume fraction of Cu nanoparticles. Bouzid et al. [5] have conducted a numerical study of mixed convection within a 3D L-cavity filled with hybrid-nanofluids. simulations were carried out for two cazes of the block's positions (VB) and (HB). The results showed that, regardless of the Richardson number and in both configurations (vertical block, VB, and horizontal block, HB), the total Nusselt number rose as the Reynolds number and the particle volume fraction increased. However, an exception was noted in the HB configuration: when the particle volume fraction was 0% and the Reynolds number was 840 or higher, the trend did not hold. Additionally, when the heated block was repositioned from the HB configuration to the VB configuration, heat transfer significantly improved by 51.16%. The comparison between the two configurations (VB and HB) yielded some fascinating results.

Bouzid et al. [6] have extended their research to analyse the magneto_Hydrodynamic combined convection of a hybrid nanfluid inside a L enclosure. The investigation comes to the conclusion that the magnetic field inclination (γ), nanoparticle concentration (\emptyset), and Hartman number (Ha) all have a substantial impact on the thermal and flow fields. Higher magnetic strength and nanoparticle volume percentage generally improve fluid flow, however as the angle of inclination of the magnetic field grows, fluid flow decreases. Temperature distribution is greatly influenced by the Hartman number, even though it is less sensitive to changes in γ and \emptyset . A higher Reynolds number (Re) and a higher Ha significantly improve heat transfer performance. A Richardson number of 0.1, a particle volume fraction of 4%, a Hartman number of 100, a magnetic field tilt of 15°, and a Reynolds number greater than 700 are the ideal parameters for optimizing the heat transfer rate.

Kumar et al. [7] used a hybrid nanofluid made of MWCNT and nanoparticles of Fe3O4 contained in water to conduct a numerical research on the upsurge of combined convection heat transfer across a heated block in a lid-driven hollow. The highest heat transmission improved of 32% occurred at a nanoparticle size of 0.1%, and a Richardson number of Ri = 1 demonstrated that the hybrid nanofluid consistently outperformed the mono nanofluid (using either MWCNT or Fe3O4 alone). The study came to the conclusion that the magnetic characteristics of Fe3O4 and the high thermal conductivity of MWCNT worked in concert to disturb the thermal boundary layer surrounding the obstruction and increase thermal transport efficiency.

A greater Reynolds number and a larger concentration of nanoparticles enhance forced convection and boost thermal conductivity, which enhances fluid circulation and heat transfer efficiency generally, according to a research by Siadi et al. [8]. Additionally, the heating block's size and placement are carefully considered, greatly enhancing thermal management in constrained areas, such as those seen in electronic cooling applications.

A numerical study by Abbasi et al. [9] examined the combined impact of mixed convection and a non-uniform magnetic field on the thermodynamic efficiency of a CuO-water nanofluid in a separated hollow with a conductive hot obstruction. A number of characteristics were examined in the study, such as barrier thermal insulation, electromagnetic field direction, and Hartmann number (Ha). According to their findings, a horizontal electromagnetic field may inhibit the convectional circulation in the nanofluid, resulting in a 15% decrease in the average Nusselt number for high Hartmann numbers (Ha > 50) because of the dominant Lorentz force. On the other hand, in certain configurations, the magnetic field was shown to arrange the flow field at lower Hartmann numbers (Ha < 20), marginally improving heat transmission.

While numerous studies have explored various hollow mixed convection geometries and with differing boundary conditions, there has been limited focus on mixed convection within L-cavities featuring a heating block. This study aims to bridge that gap by examining tis specific optimal geometry while taking into account a range of scenarios with varying flow and temperature conditions in order to maximizes heat transfer efficiency in the design of thermal engineering equipment.

1. PROBLEM FORMULATION

In a three-dimensional Enclosure, mixed convection : a mix of forced and natural convection is computationally analyzed in this study. The cavity has a heated block (a=L/6 and b=L/4) in the middle of the left wall localized by (b = L/2). The fluid "copper-water nanofluid " get's within the enclosure throw a section in the left of top wall (w = L/2), and evacuated throw a section at the bottom of the right wall . The enclosure dimension are $L\times L\times L$ As depicted in Figure 1 :

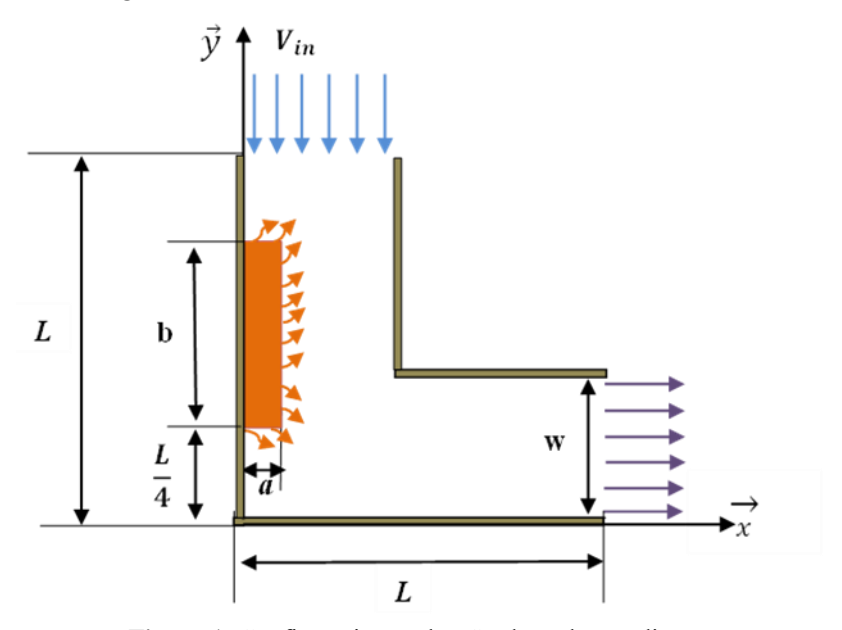


Figure 1. Configuration under Study and co-ordinates

2. NUMERICAL SCHEME AND MATHEMATICAL MODELING

As illustrated by Figure 1, this research is set up with a three-dimensional L hollow filled with a copper/water nanofluid that is impacted by floating effects. A heated obstruction is placed on the left wall of this L-cavity, which has completely adiabatic walls. The flow is considered to be constant, laminar, and three-dimensional, and radiation effects are not included in this analysis. The nanofluid is incompressible and behaves Newtonianly. The characteristics of the base fluid and the nanoparticles are listed in Table 1.

Property	Water	Copper (Cu)
β (K ⁻¹)	21× 10 ⁻⁵	1.67× 10 ⁻⁵
ρ (kg. m- ³⁾	997.1	8933
σ(Ω . m ⁻¹)	5.5×10^{-6}	5.96× 10 ⁻⁷
k (W. m-1. K ⁻¹)	0.613	401
Cp (J. kg ⁻¹ . K ⁻¹)	4179	385

Table 1. Properties of Nanofluids [14]

Density perturbations are estimated employing the Boussinesq approach. The mathematical equations that underlie these hypotheses can be constructed as outlined in reference [10].

$$\frac{\partial u}{\partial x} + \frac{\partial w}{\partial y} + \frac{\partial v}{\partial z} = 0 \tag{1}$$

$$\frac{\partial(uu)}{\partial x} + \frac{\partial(vu)}{\partial y} + \frac{\partial(wu)}{\partial z} = -\frac{1}{\rho_{vol}} \frac{\partial p}{\partial x} + v_{nf} \left(\frac{\partial^2 u}{\partial x^2} + \frac{\partial^2 u}{\partial y^2} + \frac{\partial^2 u}{\partial z^2} \right)$$
(2)

$$\frac{\partial(uv)}{\partial x} + \frac{\partial(vv)}{\partial y} + \frac{\partial(wv)}{\partial z} = -\frac{1}{\rho_{nf}} \frac{\partial p}{\partial y} + v_{nf} \left(\frac{\partial^2 v}{\partial x^2} + \frac{\partial^2 v}{\partial y^2} + \frac{\partial^2 v}{\partial z^2} \right) + \frac{(\rho\beta)_{nf}}{\rho_{nf}} (3) (T = T_{ref})$$

$$\frac{\partial(uw)}{\partial x} + \frac{\partial(vw)}{\partial y} + \frac{\partial(ww)}{\partial z} = -\frac{1}{\rho_{nf}} \frac{\partial p}{\partial z} + v_{nf} \left(\frac{\partial^2 w}{\partial x^2} + \frac{\partial^2 w}{\partial y^2} + \frac{\partial^2 w}{\partial z^2} \right) \tag{4}$$

$$\frac{\partial(uT)}{\partial x} + \frac{\partial(vT)}{\partial y} + \frac{\partial(wT)}{\partial z} = \alpha_{nf} \left(\frac{\partial^2 T}{\partial x^2} + \frac{\partial^2 T}{\partial y^2} + \frac{\partial^2 T}{\partial z^2} \right)$$
 (5)

The boundary conditions are.

Property	Property Velocity		
The outlet	$\frac{\partial u}{\partial x} = 0 ; \frac{\partial v}{\partial y} = 0 ; \frac{\partial w}{\partial z} = 0$	$\frac{\partial T}{\partial n} = 0$	
The Obstacle	u=v=w=0	$\frac{\partial T}{\partial \mathbf{m}'} = -\frac{q''}{K_{nf}}$	
The inlet	$v = v_{in}; u = w = 0$	$T = T_c$	
The remaining surfaces	u=v=w=0	$\frac{\partial T}{\partial m} = 0$	

Table 2. The boundary Conditions

Where n, m' and m are normal direction to the considered outlet, wall and obstacle respectively. The properties of the nanofluid are specified by the succeeding equations.

The nanofluid's density:

$$\rho_{nf} = \phi_p \rho_P + (1 - \phi) \rho_f \tag{6}$$

The capacitance's heat is calculated as:

$$(\rho C_p)_{nf} = \phi_p(\rho C_p)_P + (1 - \phi)(\rho C_f)_f \tag{8}$$

The thermal's expansion coefficient thermal is expressed as:

$$\beta_{nf} = \phi_p \beta_P + (1 - \phi) \beta_f \tag{9}$$

The nanofluid's diffusivity is given as:

$$\alpha_{nf} = \frac{K_{nf}}{(\rho C_p)_{nf}} \tag{10}$$

The thermal's conductivity is determined as:

$$\frac{K_{nf}}{K_f} = \frac{K_p + 2K_f - [2\phi(K_f - K_p)]}{K_p + 2K_f + [\phi(K_f - K_p)]}$$
(11)

The nanofluid's viscosity is stated as:

$$\mu_{nf} = \frac{\mu_f}{(1 - \phi_n)^{2.5}} \tag{12}$$

Seeing the boundaries:

$$X = \frac{x}{H}, Z = \frac{z}{H}, Y = \frac{y}{H}, U = \frac{u}{V_{in}}, W = \frac{w}{V_{in}}, V = \frac{v}{V_{in}},$$

$$\theta = \frac{(T - T_C)}{q'' H} K_{nf} \text{ and } P = \frac{p}{\rho_{nf} V_{in}^2}$$
(13)

The non-dimensional formulas that govern are outlined below:

$$\frac{\partial U}{\partial X} + \frac{\partial V}{\partial Y} + \frac{\partial W}{\partial Z} = 0 \tag{14}$$

$$U \frac{\partial(U)}{\partial X} + U \frac{\partial(V)}{\partial Y} + U \frac{\partial(W)}{\partial Z} = -\frac{\partial P}{\partial X} + \frac{1}{Re} \left(\frac{v_{nf}}{v_f}\right) \left(\frac{\partial^2 U}{\partial X^2} + \frac{\partial^2 U}{\partial Y^2} + \frac{\partial^2 U}{\partial Z^2}\right) \tag{15}$$

$$V \frac{\partial(U)}{\partial X} + V \frac{\partial(W)}{\partial Z} + V \frac{\partial(V)}{\partial Y} = -\frac{\partial P}{\partial Y} + \frac{1}{Re} \left(\frac{v_{nf}}{v_f}\right) \left(\frac{\partial^2 V}{\partial X^2} + \frac{\partial^2 V}{\partial Y^2} + \frac{\partial^2 V}{\partial Z^2}\right) + \frac{\partial^2 V}{\partial Z^2} + \frac{\partial$$

Where:

$$R_i = \frac{G_r}{R_e}$$
, $R_e = \frac{V_{in}H}{V_f}$, $Pr = \frac{V_f}{\alpha_f}$ and $G_r = \frac{g\beta_f H^3 \Delta T}{{V_f}^2}$ are respectively

Richardson, Reynolds, Prandtl and Grashof numbers.

The non-dimensional boundary conditions are:

1 Je Be unions						
Property	Velocity	Temperature				
The outlet	$\frac{\partial U}{\partial x} = 0; \frac{\partial W}{\partial z} = 0; \frac{\partial V}{\partial y} = 0$	$\frac{\partial \theta}{\partial n} = 0$				
The Obstacle	U=V=W=0	$\frac{\partial \theta}{\partial m'} = -\frac{K_{nf}}{K_f}$				
The inlet	$V = V_{in}; W = U = 0$	$\theta = 0$				
The remaining surfaces	$U=V=W=0\;;$	$\frac{\partial \theta}{\partial m} = 0$				

Table 3. Boundary conditions

Where n, m, m' are the normal direction to outlet, wal, and obstacle respectively.

The following provides the local nusselt number for each of the vertical block's five parts (S1, S2, S3, S4, and S5):

$$NU_{VS1} = \frac{q''H}{[T(x,z)_{y=\frac{1}{4}} - T_C]k} = \frac{1}{\theta(X,Z)_{Y=\frac{1}{4}}};$$

$$NU_{VS2} = \frac{q''H}{[T(x,z)_{y=\frac{1}{4}+b} - T_C]k} = \frac{1}{\theta(X,Z)_{Y=\frac{1}{4}+B}};$$

$$NU_{VS3} = \frac{q''H}{[T(y,z)_{x=a} - T_C]k} = \frac{1}{\theta(Y,Z)_{X=A}};$$

$$NU_{VS4} = \frac{q''H}{[T(x,y)_{z=\frac{1}{4}} - T_C]k} = \frac{1}{\theta(X,Y)_{Z=\frac{1}{4}}};$$

$$NU_{VS5} = \frac{q''H}{[T(x,y)_{y=\frac{3}{4}} - T_C]k} = \frac{1}{\theta(X,Y)_{Z=\frac{3}{4}}};$$

$$NU_{VS5} = \frac{q''H}{[T(x,y)_{y=\frac{3}{4}} - T_C]k} = \frac{1}{\theta(X,Y)_{Z=\frac{3}{4}}};$$

The usual description of the global Nusselt number is:

$$NU_{VG} = \sum_{i=1}^{5} NU_{VSGi} \tag{20}$$

Where NU_{VSG} , are the average Nusselt numbers for each sections, defined by:

$$NU_{VSG1} = \frac{2}{A \times L} \int_{L_{4}}^{3L_{4}} \int_{0}^{A} NU_{VS1} dX dZ :$$

$$NU_{VSG2} = \frac{2}{A \times L} \int_{L_{4}}^{3L_{4}} \int_{0}^{A} NU_{VS2} dX dZ :$$

$$NU_{VSG3} = \frac{2}{B \times L} \int_{L_{4}}^{L_{4+B}} \int_{0}^{3L_{4}} NU_{VS3} dY dZ :$$

$$NU_{VSG4} = \frac{1}{B \times A} \int_{L_{4}}^{L_{4+B}} \int_{0}^{A} NU_{VS4} dY dX :$$

$$NU_{VSG5} = \frac{1}{B \times A} \int_{L_{4}}^{L_{4+B}} \int_{0}^{A} NU_{VS5} dY dX$$

$$(21)$$

3. NUMERICAL METHOD

To solve the mathematical model, we utilized a custom-designed FORTRAN code. The underlying physics was addressed by discretizing the energy and Navier-Stokes equations using the finite volume method, originally proposed by Patankar (1980). This approach employs a power-law scheme to manage the convective terms in the equations, ensuring a precise representation of fluid dynamics.

The resultant algebraic equations were solved with the tridiagonal matrix algorithm, which allows for iterative resolution of the equation system. This iterative method plays a crucial role in achieving efficient convergence to an accurate solution.

The convergence of our numerical code was rigorously evaluated, with the assessment based on a set of specific criteria that were carefully established and consistently applied throughout the computational process.

$$\sum_{i,j,k=1}^{i \max, j \max, k \max} \frac{\left| \Phi_{i,j,k}^{n+1} - \Phi_{i,j,k}^{n} \right|}{\left| \Phi_{i,j,k}^{n} \right|} \le 10^{-5}$$
(26)

In this context, Ø denotes a dependent variable such as pressure (P), vertical velocity (W), horizontal velocity (V), longitudinal velocity (U), or temperature (T). The variable "n" refers to the iteration count, while the indices "i," "j," and "k" represent the grid locations along the respective axes.

3.1 Grid Size Independency

Selecting the optimal grid size is fundamental in computational simulations, as it affects both accuracy and computational resource allocation. To ensure grid independence, the Nusselt number was evaluated across a range of uniform grid sizes, with the corresponding results presented in Table 2. This analysis revealed that a 81×81×81 grid offered an appropriate balance between result accuracy and computational efficiency, aligning well with the current study's objectives.

Further refinement to a 91×91×91 grid yielded only a minimal difference in the Nusselt number-approximately 1.18%. This marginal variation indicates that additional grid refinement has a negligible impact on system performance, validating the suitability of the 81×81×81 grid for the given research. The results from this examination provide robust support for the selected grid size, offering assurance in the precision of the derived outcomes while optimizing computational resource use.

Grid Size	41×41×41	61×61×61	71×71×71	81×81×81	91×91×91
Nusselt number	5.18	5.28	5.40	5.99	6.11

Table 4. Grid size tests

3.2 Code Validation

To validate the reliability of our computational code, we conducted a comparative analysis of the Nusselt numbers obtained from our simulations against those reported in earlier studies by Ravnik [12]. The results of this comparison are summarized in Table 3, which accounts for a range of Rayleigh numbers.

Similarly, as depicted in Figure 2, we compared the thermal distribution obtained from our modeling approach to the results documented by Moraga et al. [13]. The comparison between our results and those of the earlier studies by Ravnik [12] and Moraga et al. [13] demonstrates a high degree of consistency, with an overall discrepancy of approximately 3.24%. This finding suggests that our computational algorithm successfully captures the essential characteristics of the problem and generates outcomes consistent with established literature.

	Wa	Vater		Water + Cu <i>φ</i> = <i>0.1</i>			Water + Al_2O_3 $\varphi = 0.1$		
R a	Prese nt work	Ref Ravn ik [12]	differen ce	Prese nt work	Ref Ravn ik [12]	differen ce	Prese nt work	Ref Ravn ik [12]	differen ce
10	1.082	1.071	1.02%	1.381	1.363	1.32%	1.362	1.345	1.26%
10	2.114	2.078	1.73%	2.257	2.237	0.89%	2.187	2.168	0.87%
10	4.631	4.510	2.68%	5.047	4.946	2.04%	4.904	4.806	2.03%
10	9.325	9.032	3.24%	10.38	10.08	2.97%	10.09	9.817	2.78%

Table 5. Comparison of Nusselt number with those of Ravnik [12]

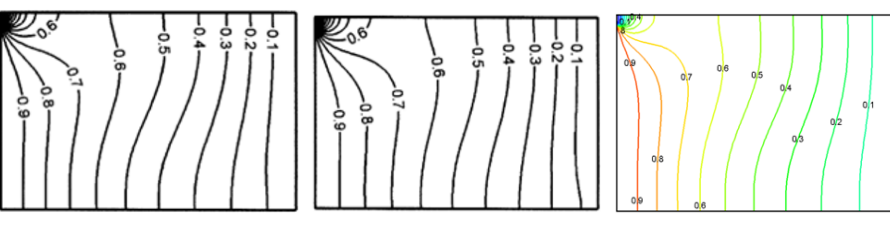


Figure 2. Comparison of the isotherms acquired at Z = 0.5 plane with those obtained by Moraga et al. [13] when Ri = 10 and Re = 5

4. RESULTS AND DISCUSSION

This study aims to investigate the effects of geometric and thermal parameters on fluid flow behavior and heat transfer within a three-dimensional L-shaped cavity. The analysis focuses on several key aspects, including the global Nusselt number, streamlines, temperature distribution, and flow patterns, across a broad range of thermal conditions. The parameters explored encompass "Richardson numbers" $(0.1 \le Ri \le 10)$, Reynolds numbers $(10 \le Re \le 200)$, and the volume fraction of nanoparticles $(0\% \le \emptyset \le 4\%)$.

Figure 3 displays the temperature distribution and flow patterns within a three-dimensional cavity under specific conditions: Reynolds number (Re) of 100, Richardson number (Ri) of 0.1, and 4% volume fraction of nanoparticles (\emptyset). The illustration depicts the movement of fluid from the partition towards the exit, resulting in continuous evacuation of heat from the cavity through convection. To provide a comprehensive view of the temperature distribution in the cavity, various planes were examined. Consequently, we have selected the plane corresponding to Z=1/2, intersecting the midpoint of component 1 perpendicularly, as it offers a representative depiction of flow and heat transfer within the cavity. The presented results stem from simulations conducted across a range of Reynolds numbers (10 to 200), Richardson numbers (0.1 to 10), and nanoparticles volume fractions (0% to 5%).

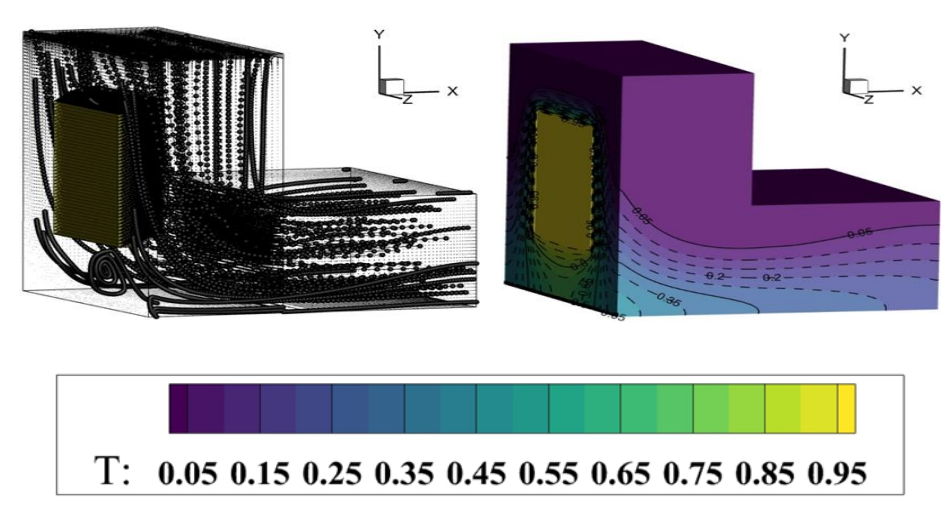


Figure 3. Temperature distribution (right) and flow patterns (left), for Re = 100, Ri = 0.1 and $\emptyset = 4\%$

4.1. Effect of the Nanoparticle

Figure 4. depicts an analysis of the thermal field and flow pattern for a fixed Reynolds number (Re = 100) and Richardson number (Ri = 0.1) along with various nanoparticle volume fractions ($\emptyset = 0\%$, 3%, and 5%).

The majority of stream appears at $\emptyset = 0\%$, with jets maintaining a consistent path from the heating block's top layer to the enclosure's bottom area with just tiny variations at the ends. Due to the very limited nature of the thermal field in this setup, the isotherms show a concentrated distribution of increased temperatures close to the heating block.

The fluid experiences a more pronounced redirection when it contacts with the cavity's bottom border when the nanoparticle volume percentage rises ($\emptyset \ge 0\%$). The clustering of higher temperatures in this area is highlighted by the related isotherms, which show a layered and concentrated structure surrounding the heating block. The isotherms at lower and intermediate temperatures, on the other hand, are almost parallel to each other in the remaining cavity portions, indicating a clear thermal structure in these regions. This increased volume percentage causes more complex fluid dynamics, which impact the system's overall temperature distribution as well as the flow's rerouting.

In comparison to a scenario of $\emptyset = 0\%$, the improvement in heat transfer is still restricted when the concentration of nanofluid particles is raised to $\emptyset = 3\%$ at a Reynolds number of Re = 100. When metallic nanoparticles are added to the base fluid and interact with the heated block and incoming flow, the fluid density and particle mobility are not changed enough to have a noticeable thermal impact. The careful balance between inertial forces and nanoparticle characteristics is responsible for the noticeable increase in fluid velocity that occurs at the same time. As the particle volume fraction rises, the flow field also shows the appearance of a little circular vortex beneath the block.

Although there is a more noticeable increase in heat transmission, the thermal and flow fields behave similarly to those at $\emptyset = 3\%$ at a nanoparticle volume fraction of $\emptyset = 5\%$. The main cause of this improvement is the increased contact between the heated block and the entering fluid, which has a major impact on fluid density and encourages particle mobility.

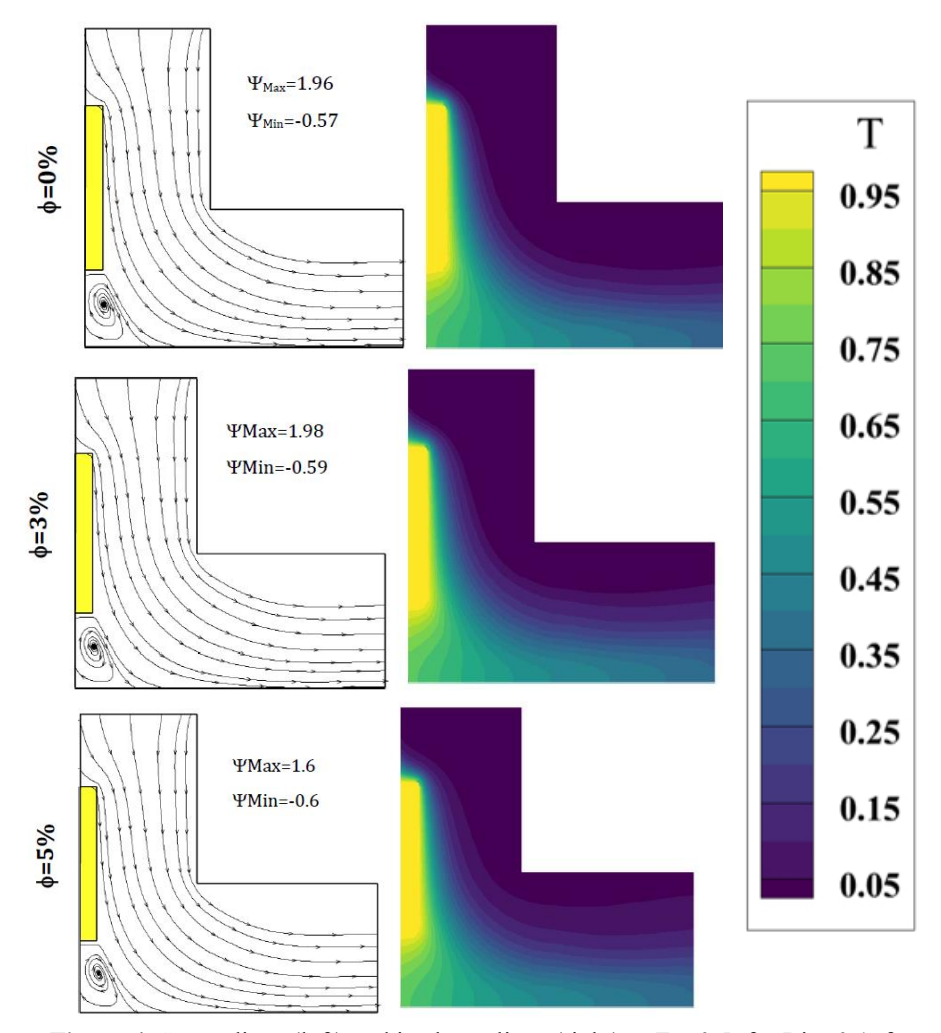


Figure 4. Streamlines (left) and isotherm lines (right) at Z=0.5, for Ri=0.1, for Re=100, and for various volumes fraction of nanoparticles (0%, 3% 5%)

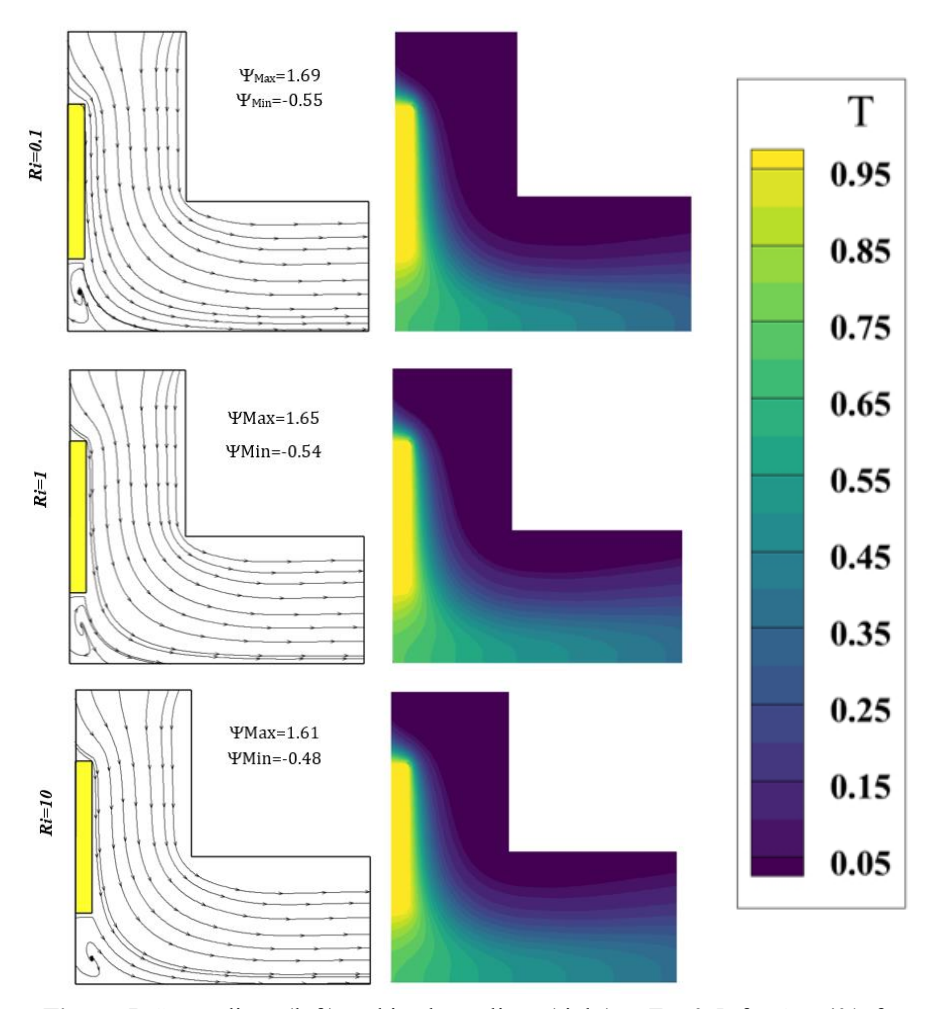


Figure 5. Streamlines (left) and isotherm lines (right) at Z = 0.5, for $\emptyset = 4\%$, for Re=100, and for various Richardson numbers Ri = 0.1, 1 and 10

Higher volume fractions cause the temperature distribution to become more concentrated around the heated block before gradually moving in the direction of the cavity exit. The buoyancy forces produced by the heated block and the oncoming cold flow work together to cause this change.

4.2 Effect of Richardson Number

As shown in Figure 5, the flows and isotherms are analyzed in the Z=0.5 plane to assess the efficiency of heat transfer and patterns of flow. Comparing the fluid and thermal dynamic behavior for various Richardson numbers (Ri) is the aim of the study. Using the Reynolds number set at Re = 0.1 and the nanoparticle volume fraction of the copper–water nanofluid constant at $\emptyset=4\%$, a series of simulations were run along the range $0.1 \le Ri \le 10$.

When the fluid is moving toward the outlet, the unhindered streamlines linked to externally pushed flow span the whole top surface of the block at a Richardson number of Ri=0.1, creating a spinning vortex at the bottom of the enclosure. Because inertial forces outweigh buoyancy effects, the flow is free to circulate and transfer heat energy along the hollow, creating this vortex. The previously noted counterclockwise vortex at the bottom drastically decreases when the Richardson number is raised to Ri=1. This decrease is mostly caused by the stability of mixed convection, which changes the fluid density and the mobility of the suspended metal nanoparticles by making buoyancy forces more significant than inertial forces. Furthermore, the interaction between the entering flow and the metal particles in the base fluid modifies the flow patterns because the nanoparticles redistribute momentum and increase local viscosity, which weakens the vortex. As the Richardson number rises, the flow becomes more ordered and convective transport becomes less noticeable, demonstrating the system's delicate balance between forced and spontaneous convection.

The flow lines show a significant decrease in fluid velocity and the total elimination of the vortex that was previously located at the bottom of the heated block when the Richardson number is increased further to Ri = 10. Conduction now predominates over convection throughout the enclosure, signifying a change in the major heat transport mechanism. The uniform distribution of thermal gradients in areas less affected by fluid motion is reflected in the substantially symmetrical pattern formed by the isotherms corresponding to lower temperatures running almost parallel to the heated block. On the other hand, there is a discernible asymmetry in the isotherms around the flow-oriented heated block, indicating localized thermal disturbances and the residual effects of small convective currents.

The intricate relationship between dominant conductive heat transmission and residual flow motion is demonstrated by this mix of symmetrical low-temperature zones and asymmetric high-temperature sections. Additionally, the temperature field becomes increasingly stratified overall, with the heated block containing the majority of the high-temperature area and the rest of the cavity approaching a quasi-steady thermal state.

4.3 Heat Transfer

To evaluate the heat transfer performance of the studied configuration, the variations of the global average Nusselt number on the heating surfaces of the block are examined as a function of nanoparticle volume fraction (\emptyset) and Richardson number (Ri) for different Reynolds numbers, as illustrated in Figure 6. The results indicate that the Nusselt number generally increases with both nanoparticle volume fraction and Reynolds number across all considered Richardson numbers. However, at a low Reynolds number (Re = 10), the increase in Nusselt number with rising nanoparticle concentration is modest (8% enhancement). This behavior is attributed to the weak interaction between inertial and buoyancy forces, resulting in a slow development of mixed convection.

Moreover, the addition of metallic nanoparticles has a limited effect on the base fluid's density and particle mobility, and their interaction with the heated block and incoming flow does not significantly enhance convective transport, so heat transfer near the heating block remains largely conductiondominated.

Additionally, decreasing the Richardson number substantially improves the cooling of the heated block by 12.5 % enhancement when Re = 10 and 17 % increase when Re = 200. This enhancement is due to the more effective exchange between the incoming external flow and the heated surface, which accelerates the onset and intensity of mixed convection, thereby promoting higher heat transfer rates.

Furthermore, increasing the nanoparticle portion from 0 % to 5 % lead to and enhancement of 30 % when Ri and Re are set respectively at 0.1 and 200.

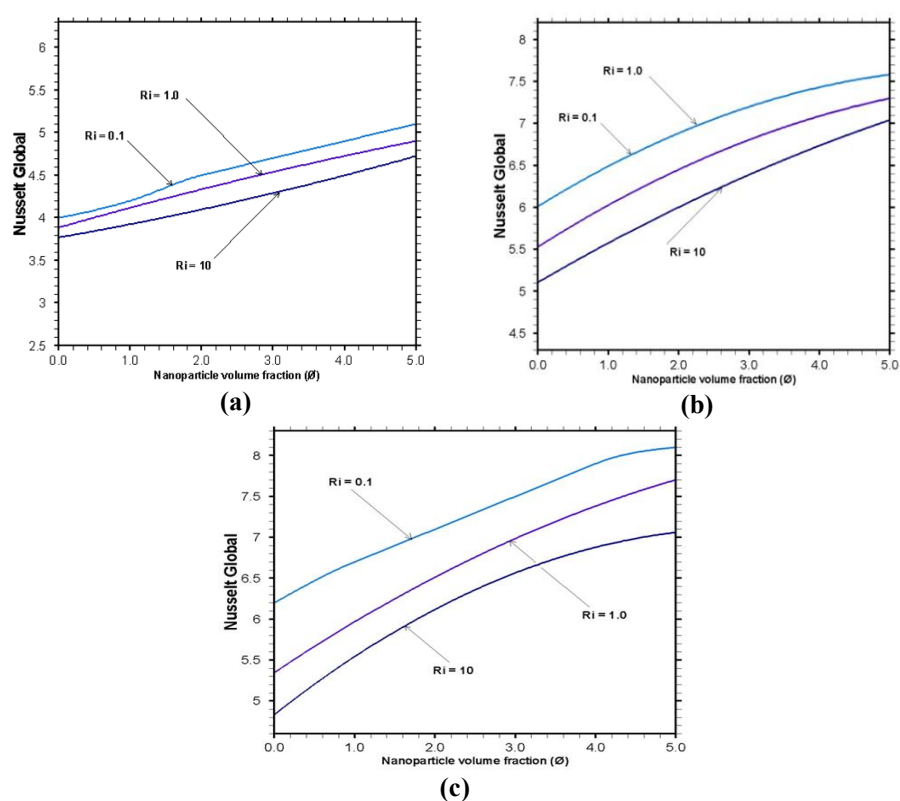


Figure 6. Variation of the global average Nusselt number for different Reynolds numbers (a) Re = 10, (b) Re = 100, and (c) Re=200, with Nanoparticle volume fraction (Ø) number and different Richardson number (Ri)

CONCLUSION

We used a finite volume model to examine the heat transfer inside a three-dimensional L-cavity with a heated block inside. This numerical investigation of mixed convection phenomena took into account a number of significant variables, such as the Reynolds number, Richardson number, and the volume fraction of (Cu) nanoparticles. The main conclusions drawn from our study are outlined here.

- Increasing the nanoparticle concentration enhances heat transfer, particularly at moderate to high Reynolds numbers, by locally increasing thermal energy near the heated block and slightly modifying flow structures.
- Higher Reynolds numbers strengthen forced convection, producing stronger vortices, higher fluid velocities, and more uniform temperature distribution, while low Re leads to conduction-dominated heat transfer.
- Low Ri favors convection-dominated flow with vigorous vortices, moderate Ri promotes mixed convection, and high Ri suppresses vortices, leading to conduction-dominated heat transfer with stratified temperature fields.
- The size, strength, and location of vortices are strongly influenced by Re, Ri, and nanoparticle content; temperature distribution becomes more uniform with stronger convection, while high Ri and low Re result in stratified, conduction-driven patterns.
- Maximum heat transfer occurs at low Ri (Ri = 0.1), high Re (Re = 200), and moderate-to-high nanoparticle fractions (Ø = 5 %) by 30% enhancement, reflecting the combined effects of enhanced fluid motion, buoyancy forces, and nanoparticle-induced thermal conductivity improvements.

MODERN APPROACHES IN APPLIED MECHANICAL ENGINEERING

Nomenclature						
A,B	Dimensionless Heat block, []	P	Dimensionless pressure, []			
C_P	"Specific heat capacity", [J. Kg ⁻¹ . K ⁻¹]	Pr	Prandtl number, []			
G	Gravitational hurrying, [m. s ⁻²]	q''	Heat flux, [W.m ⁻²]			
Gr	Grashof number, []	Re	Reynoldsnumber, []			
H	Characteristic length, [m]	Ri	Richardson number, []			
K	"Thermal conductivity", [W. m ² . K ⁻¹]	T	Temperature, (K)			
L	Dimensionless heat block, []	<i>U, V,</i>	Dimensionless velocity, []			
		W				
NU	Nusselt number, []	<i>X</i> , <i>Y</i> , <i>Z</i>	Dimensionless coordinates,			
P	Pressure, (Pa)					
Greek symbols						
α	Thermal diffusivity, [m ² .s ⁻¹]	C	cold			
β	"Coefficient of Thermal expansion"	F	Fluid			
μ	Dynamic viscosity, [Kg.m ⁻¹ .s ⁻¹]	G	Global			
ν	Kinematic viscosity, [m.s ⁻¹]	Н	horizontal			
Ø	Solid volume fraction of	Hnf	Hybrid-nanofluid			
	nanoparticles, []	,	-			
θ	Dimensionless temperature, []	Pi	Considered particle			
ρ	Density, [Kg.m ⁻³]	S	Solid nanoparticle			
		t	Тор			
Subscrip	Subscripts					
В	Bottom	V	Vertical			

REFERENCES

- Abbasi, Z., Selimefendigil, F., & Oztop, H. F. (2024). Numerical analysis of magnetic field impact on mixed convection of CuO-water nanofluid with an inner conductive obstacle in a partitioned cavity. Journal of Magnetism and Magnetic Materials, 591, 171735.
- Armaghani, T., Sadeghi, M. S., Rashad, A. M., Mansour, M. A., Chamkha, A. J., Dogonchi, A. S., & Nabwey, H. A. (2021). MHD mixed convection of localized heat source/sink in an Al2O3-Cu/water hybrid nanofluid in L-shaped cavity. Alexandria Engineering Journal, 60(3), 2947-2962.
- Belarche, L., Abourida, B., Doghmi, H., Sannad, M., & Ouzaouit, M. (2021). Three-dimensional simulation of controlled cooling of electronic component by natural and mixed convection. Thermal Science, 25(4 Part A), 2565-2577.
- Belarche, A. S. L., Abourida, B., & Bouzid, K. Mixed Convection Investigation Of A Heating Block Within A Lid-Driven Cubic Cavity Filled With Nanofluid. International Journal on Technical and Physical Problems of Engineering (IJTPE), Issue 60, Vol. 16, No. 3, pp. 203-212, September 2024.
- Bouzid, K., Belarche, L., Abourida, B., Siadi, A., & Nouari, S. (2024). Numerical investigation of mixed convection inside a 3-D L-shaped cavity filled with hybrid-nanofluids in the presence of a heating block. Thermal Science, 28(4 Part B), 3235-3252.
- Bouzid, K., Belarche, L., Abourida, B., & Siadi, A. Numerical Investigation Of Mhd Hybrid Nanofluid Mixed Convection Within A Three-Dimensional L-Shaped Cavity. International Journal on Technical and Physical Problems of Engineering (IJTPE), Issue 60, Vol. 16, No. 3, pp. 172-182, September 2024.
- Gorla, R. S. R., Siddiqa, S., Mansour, M. A., Rashad, A. M., & Salah, T. (2017). Heat source/sink effects on a hybrid nanofluid-filled porous cavity. Journal of Thermophysics and Heat Transfer, 31(4), 847-857.
- Hssain, M. A., Mir, R., & El Hammami, Y. (2020). Numerical simulation of the cooling of heated electronic blocks in horizontal channel by mixed convection of nanofluids. Journal of Nanomaterials, 2020(1), 4187074.

- Kumar, P., Sharma, K., & Nguyen, T. K. (2024). Enhanced cooling of a heated block in a lid-driven square cavity using hybrid MWCNT-Fe3O4/water nanofluid under mixed convection. International Communications in Heat and Mass Transfer, 151, 107201.
- Moraga, N. O., & Lopez, S. E. (2004). Numerical simulation of three-dimensional mixed convection in an air-cooled cavity. Numerical Heat Transfer, Part A: Applications, 45(8), 811-824.
- Nouari, S., Bara, E., Lafdaili, Z., EI-Hamdani, S., Bendou, A., & Doghmi, H. (2022). Unsteady numerical investigation of nanofluid mixed convection within a cubic cavity with periodic motion of double oscillatory walls. International Journal of Numerical Methods for Heat & Fluid Flow, 32(11), 3452-3469.
- Patankar, S. V., Numerical heat transfer and fluid flow, McGraw-Hill,. New York., USA, 1980.
- Ravnik, J., Škerget, L., & Hriberšek, M. (2010). Analysis of three-dimensional natural convection of nanofluids by BEM. Engineering Analysis with Boundary Elements, 34(12), 1018-1030.
- Wang, L., Djebali, R., & Godson, L. (2024). Thermohydraulic performance of SiO2-water nanofluid in a partitioned cavity with a rotating cylinder for electronic cooling applications. Case Studies in Thermal Engineering, 55, 104112.

